

ELASTIC STABILIZATION OF ARRAYS  
OF PRECIPITATES IN  
Al-4%Cu ALLOY

by

VUKO PEROVIC, Dipl. Ing.

A Thesis

Submitted to the Faculty of Graduate Studies  
in Partial Fulfilment of the Requirements  
for the Degree  
Master of Engineering

McMaster University

September 1976

MASTER OF ENGINEERING  
(Metallurgy)

McMASTER UNIVERSITY  
Hamilton, Ontario

TITLE: Elastic Stabilization of Arrays of Precipitates  
in Al-4%Cu Alloy

AUTHOR: Vuko Perovic, Dipl. Ing.

SUPERVISOR: Dr. G. R. Purdy

NUMBER OF PAGES: (viii); 73

SCOPE AND CONTENTS:

The elastic interaction of the new phase coherent particles with tetragonal distortion is considered. The analysis shows that the elastic energy may be minimized by the formation of regular tridimensional arrays.

Studies of the variations of the interaction energy of the Tyapkin array with respect to displacements and volume perturbation of the particles (in the finite approximation) lead to the conclusion that the periodic distribution is stable.

## ACKNOWLEDGMENTS

I wish to express my gratitude to Dr. G. R. Purdy for suggesting the topic of research and for his encouragement and help throughout the study. Special thanks are due to Dr. L. M. Brown and Dr. J. D. Embury for discussions which proved most helpful. Thanks are also extended to many of the faculty, technical staff and graduate students, and to the National Research Council of Canada who provided financial support.

## TABLE OF CONTENTS

	<u>Page</u>
CHAPTER I INTRODUCTION	1
CHAPTER II THEORETICAL BACKGROUND AND REVIEW OF PREVIOUS WORK	4
II. 1. The Role of Elastic Energy in Phase Transformations in the Solid State	4
II. 2. Elastic Stabilization of Arrays of Precipitates against Ostwald Ripening	18
II. 3. Previous Work on Al-4%Cu	21
II. 4. An Approximation for the Strain Field of a Disc-shaped G.P. Zone	25
II. 5. Interaction between Pairs of Dislocation Loops - The Infinitesimal Approximation -	29
CHAPTER III INTERACTION AMONG FINITE PRECIPITATES	33
CHAPTER IV CONCLUSIONS AND SUGGESTIONS FOR FUTURE WORK	53
IV. 1. Conclusions	53
IV. 2. Suggestions for Future Work	56
APPENDIX COMPUTATION OF INTERACTION ENERGIES	58
REFERENCES	71

FIGURE CAPTIONS:

- Fig. 1. Log - log plot of mean diameter of the  $\Theta''$  and  $\Theta'$  particles against time.
- Fig. 2. The structure of the  $\Theta''$  precipitate.
- Fig. 3. The misfit in the c direction is taken by elastic displacements in the matrix.
- Fig. 4. The structure of the  $\Theta'$  precipitate.
- Fig. 5. Pure prismatic infinitesimal dislocation loop.
- Fig. 6. Parallel prismatic dislocation loops,  
 $b_1 \parallel b_2, n_1 \parallel n_2$ .
- Fig. 7. Perpendicular prismatic dislocation loops,  
 $b_1 \parallel b_2, n_1 \parallel b_1, n_2 \parallel b_2$ .
- Fig. 8. Interaction energy of two square shaped (  $d=10$  units) particles when they are mutually parallel (face-face configuration) as a function of separation. The broken line indicates the interaction of infinitesimal precipitates of the same strength.  $D$  is the centre to centre distance; each unit represents  $1/10$  of the length of the particle \*.
- Fig. 9. Interaction energy of two squared shaped (  $d=10$  units) particles when they are mutually parallel (edge-edge configuration) as a function of separation.

---

\*  $D$  has the same meaning in the all other figures in which it appears.

Fig.10. Interaction energy of two square shaped particles when they are mutually perpendicular (edge-face configuration) as a function of separation. The broken line indicates the interaction of infinitesimal precipitates of the same strength.

Fig.11. Interaction energy of two square shaped particles when they are mutually perpendicular (edge-face configuration) as a function of separation. The broken line indicates the interaction of infinitesimal precipitates of the same strength.

Fig.12. The Tyapkin array.

Fig.13. The total elastic energy of the Tyapkin array per central plate versus the distance between the plates. The energy was calculated between the central plate and the plates enclosed by the sphere of radius of 50 units.

Fig.14. The total elastic energy of the Tyapkin array per central plate versus the distance between the plates enclosed by the sphere of radius of 50 and 100 units.

Fig.15. The total elastic energy of the Tyapkin array versus number of precipitates calculated for  $1/8$  of the sphere. The distance between the particles is 15 units.

Fig.16. The total elastic energy of the Tyapkin array per central plate in the infinitesimal

approximation versus the distance between the plates. The energy was calculated between the central plate and the plates enclosed by the sphere of radius of 50 units.

Fig.17. The total elastic energy of the Tyapkin array as a function of the virtual displacement of the central plate along  $x$  ( $y$ ) direction. Radius of the sphere is 50 units and the distance (centre to centre) is 15 units.

Fig.18. The total elastic energy of the Tyapkin array as a function of the displacement of the central plate along  $z$  direction. Radius of the sphere is 50 units and the distance is 15 units.

Fig.19. The total elastic energy of the Tyapkin array in infinitesimal approximation as a function of the displacement of the central plate along  $x$  ( $y$ ) direction. Radius of the sphere is 50 units and the distance is 15 units.

Fig.20. The total elastic energy of the Tyapkin array in infinitesimal approximation as a function of the displacement of the central plate along  $z$  direction. Radius of the sphere is 50 units and the distance is 15 units.

Fig.21. The configuration of the cubic sublattices.

Fig.22. The  $\langle 1213 \rangle$  array.

Fig.23. The  $\langle 1332 \rangle$  array.

- Fig.24. The total elastic energies per plate of the Tyapkin array and of the  $\langle 1332 \rangle$  array of precipitate in location "A" as a function of separation. Radius of the sphere is 50 units and the distance is 15 units.
- Fig.25. The change of the elastic energy due to the volume changes between the pair of precipitates in the edge-face configuration (x, y directions).
- Fig.26. The change of the elastic energy due to the volume changes between the pair of precipitates in the face-face configuration (z direction).
- Fig.27. A schematic representation of the positions of the nearest neighbours around perturbed precipitates 1' and 2' in the Tyapkin array.
- Fig.28. The elastic energy change of the Tyapkin array as a function of the variation of the volume of the central plate and its first neighbour in the z direction. Radius of the sphere is 60 units and the distance is 15 units.
- Fig.29. The periodic arrangement of  $\Theta'$  precipitates in Al-4 %Cu alloy (courtesy of C. Sargent).



## CHAPTER I

### INTRODUCTION

The phenomenon of clustering (or zone formation) so essential to precipitation hardening is the method by which an alloy can lower its free energy at low temperature after quenching.

The total free energy of a quenched and aged alloy may be regarded as the sum of the free energies of the matrix and precipitate phases, the free energy of the interfaces (coherent or incoherent) separating the phases, and the elastic strain energy of the matrix and precipitates.

While the chemical free energies of the matrix and precipitate phases generally provide the bulk of the driving force for precipitation, the elastic strain energy may significantly affect the kinetic path along which the ageing occurs. That is, the elastic strain energy is generally believed to exert a major influence upon the distribution and shape of clusters or zones. This point has been stressed recently by several authors<sup>1,9,15,36,38,39</sup>

The phase transformation in a solid is, to a large extent, controlled by the elastic deformation in the matrix. Three types of coupling are possible, i.e., coherent, partly coherent and completely incoherent. From the microscopic viewpoint, the condition of coherency means that atoms lying on either side of the two-phase

boundary which were neighbours before transformation remain neighbours after transformation also.

Coherent or semi-coherent coupling often arises during the early stages of a decomposition process, and also during a martensite transformation.

In the investigation of the coherent stage the following important questions arise:

1. What is the optimum shape of the new-phase particles to ensure minimum free energy?
2. What is the orientation of the new-phase particles relative to the crystallographic axes of the matrix?
3. What is the orientational relationship between the lattices of the two phases?
4. What is the mutual spatial distribution of the inclusions?

A complete answer to the questions posed may be obtained by considering the elastic properties of the matrix and the precipitate, the crystal geometry of the transformation and the surface tension.

As already mentioned one of the fundamental peculiarities of certain phase transitions in the solid state consists in the fact that they are often accompanied by considerable elastic deformations of the parent crystal lattice. At the same time the phase transition occurs in such a manner that at each step the loss of free energy of the system due to the deformation turns out to be minimal. The minimization of the elastic energy

is possible because of the optimal form and distribution of the inclusions of the new phase, which are coherently bound to the matrix, and also by means of the formation of epitaxial dislocations at the interphase boundaries (violation of coherence), if the possibilities of reduction of the stresses due to change of orientations and form of the inclusions are limited.

The aim of this work has been to examine the possibility that the strain energy contribution to the total driving force for precipitation may be responsible for the formation of regular arrays or lattices of plate-like precipitates.

## CHAPTER II

### THEORETICAL BACKGROUND AND REVIEW OF PREVIOUS WORK

#### II.1. The role of elastic energy in phase transformations in the solid state . 7

As a result of fluctuations in concentration and order parameters, inhomogeneities bearing a more or less random character arise in the crystal. If the lattice parameters depend strongly on composition, then from the macroscopic point of view the inhomogeneities of composition will lead to concentration stresses, inhomogeneous strains associated with these, and static displacements of the atoms in the crystal. As a result of the superposition of the fields of the displacements created by different atoms, a complex distribution of static displacements develops in the solution.

It is clear that the determination of the stresses and static displacements as functions of the coordinates of the atoms in the crystal in the above mentioned case of a complex and not completely symmetrical fluctuation distribution of stresses sources constitutes an extremely difficult problem.

The problem is greatly simplified, however, if we use the method of fluctuation waves and transform from the displacements of the atoms to their Fourier components<sup>1</sup>.

In the case of long-wave fluctuation waves we may carry out a macroscopic calculation of the static

displacement waves, based on the use of equations taken from elastic theory and not on any specific model of the crystal. The amplitudes of the displacement waves are expressed in terms of crystal characteristic which may easily be determined experimentally.

In the case of short wave fluctuations, the macroscopic approach becomes inapplicable.

For a wave-like change in concentration

$$\delta c(r) = c_k \exp(-ikr) \quad (1)$$

corresponding to the k-th fluctuation wave, the displacements and strains also vary in an wave-like manner:

$$U_{lm} = \frac{1}{2} \left[ \frac{\partial(\delta R_l)}{\partial x_m} + \frac{\partial(\delta R_m)}{\partial x_l} \right] =$$

$$= \frac{1}{2} \left[ k (n_m A_{kl} + n_l A_{km}) \right] c_k \exp(-ikr) \quad (2)$$

where  $n_l$  are the components of the unit vector  $n = k/k$  parallel to the wave vector  $k$ ,  $A_k$  the proportionality factors between the amplitudes of the static-displacement and concentration waves.

Following Khachaturyan<sup>1</sup> the elastic energy of unit volume of the new phase particle-matrix system has the form:

$$f(r) = \mathcal{G}_{ij}^0 \Theta(r) \mathcal{E}_{ij} + \frac{1}{2} \lambda_{ijklm} \mathcal{E}_{ij} \mathcal{E}_{lm} \quad (3)$$

where  $\lambda_{ijklm}$  is the elasticity modulus tensor,  $\mathcal{E}_{ij}$  is the deformation tensor,  $\Theta(r)$  is the form function equal to unity inside the inclusion and zero outside, and  $\mathcal{G}_{ij}^0$  is the tensor characterizing the crystal geometry of the transformation; twice-repeated indices everywhere denote summation.

Transforming to Fourier components, we obtain:

$$\lambda_{ijklm} k_j k_l u_m(k) = i \mathcal{G}_{ij}^0 k_j \Theta(k) \quad (4)$$

where  $u(k) = \int d^3 r u(r) \exp[-i(k,r)]$   
 $u(r)$  is the displacement of the point  $r$ , and  
 $\Theta(k) = \int d^3 r \Theta(r) \exp[-i(k,r)]$ , with the integration being taken over infinite space.

The solution of the equilibrium equation has the form:

$$U(k) = i \Theta(k) G^{-1}(k) \hat{\mathcal{G}}_0 K \quad (5)$$

where  $G^{-1}(k)$  is the Green's function of the elastic equilibrium equation. Expressing the elastic energy of the system,  $E_1 = \int d^3 r f(r)$ , in terms of Fourier components

of the integrand functions, we get:

$$E_1 = - \frac{1}{2} \int \frac{d^3 k}{(2\pi)^3} |\Theta(k)|^2 A(k) \quad (6)$$

$$\text{where } A(k) = (\hat{\epsilon}_0 k, G^{-1} \hat{\epsilon}_0 k) = (k, \hat{\epsilon}_0 G^{-1} \hat{\epsilon}_0 k) \quad (7)$$

The energy given by Eqs. 6 and 7 is counted from the state of the system at which  $\epsilon_{ij} = 0$ . The state  $\epsilon_{ij} = 0$  is stressed, and its energy is not at a minimum. The minimum elastic energy is possessed by the state with  $\hat{\epsilon}_{ij} = 0$ , when both phases are in the free state:

$$E(\hat{\epsilon}_{ij}=0) = - \frac{1}{2} \hat{\epsilon}_{ij}^0 \epsilon_{ij}^0 V = - \frac{1}{2} \lambda_{ijlm} \epsilon_{ij}^0 \epsilon_{lm}^0 V \quad (8)$$

where  $V$  is the volume of the new phase. Using Eq. 7 we obtain an expression for the elastic energy reckoned from the unstressed state, which is equal to:

$$E = E_1 - E(\hat{\epsilon}_{ij}=0) = \frac{1}{2} \lambda_{ijlm} \epsilon_{ij}^0 \epsilon_{lm}^0 V - \int \frac{d^3 k}{(2\pi)^3} A\left(\frac{k}{k}\right) |\Theta(k)|^2 \quad (9)$$

Eq. 9 expresses the elastic energy in terms of the coefficients  $\hat{\epsilon}_{ij}^0$  and  $(G^{-1})^{ij}$  which characterize the elastic properties of the transformation, and also in terms of the function  $|\Theta(k)|^2$ , which characterize the shape of the particle.

To elucidate the orientational relationship between the lattices of the phases it is necessary to find the angle of rotation of the new-phase particle relative to the matrix. The vector of local rotation,  $\varphi$ , at a point is expressed in terms of the displacement at this point by the equation:

$$\langle \varphi \rangle = \frac{1}{V} \int \frac{d^3 k}{(2\pi)^3} \left| \Theta(k) \right|^2 \left| k, G^{-1}(k) \hat{e}_0 k \right| \quad (10)$$

Equation 9 is valid if elastic moduli of the inclusions and of the matrix are equal. From the structure of Eq. 10 it follows that the orientation of the invariant plane (the orientational relationship) depends, generally speaking, on the shape of the crystal of the new phase. The formation of a single inclusion of the new phase in an infinite anisotropic continuum is accompanied by a minimum value of the elastic energy if the inclusion has the form of a thin extended plate, the normal unit vector  $k_0$  of which is determined by the condition of maximum for the quantity  $A(k/k)$ .

The answers to the questions posed can be formulated:

1. The optimum shape of a new-phase particle to ensure minimum elastic energy is that of a thin plate, with length and width much greater than its thickness.

2. The plane of this plate is perpendicular to one of the  $k_0$  vectors, thus bringing about a maximum  $A(k/k)$ .



3. The direction of magnitude of the angle of rotation of the crystallographic axes of this plate are given by Eq. 10. The invariant plane is perpendicular to the vector  $\langle \Psi \rangle$ .

For the case where the crystal geometry of the transformation is described by tensor  $\epsilon_{ij}^0$ , which has a tetragonal character, while the matrix has a cubic lattice;  $\epsilon_{11}^0 = \epsilon_{22}^0 = \Delta a/a$ ,  $\epsilon_{33}^0 = \Delta c/c$ ,  $\epsilon_{ij}^0 = 0$  when  $i \neq j$ . In that case we have:

$$\epsilon_{ij}^0 = \epsilon_0 \begin{vmatrix} 1 & 0 & 0 \\ 0 & 1 & 0 \\ 0 & 0 & 1 \end{vmatrix} + \tilde{\epsilon}_0 \begin{vmatrix} -1/2 & 0 & 0 \\ 0 & -1/2 & 0 \\ 0 & 0 & 1 \end{vmatrix} \quad (11)$$

where

$$\epsilon_0 = \frac{c_{11} + 2c_{12}}{3} \quad \epsilon_{11}^0 = \frac{c_{11} + 2c_{12}}{3} \left( -2 \frac{\Delta a}{a} + \frac{\Delta c}{c} \right)$$

$$\tilde{\epsilon}_0 = \frac{2(c_{11} - c_{12})}{3} \left( \frac{\Delta c}{c} + \frac{\Delta a}{a} \right)$$

$$\lambda_{1111} = c_{11}, \quad \lambda_{1122} = c_{12}, \quad \lambda_{1212} = c_{44}$$

For the case of a cubic lattice the matrix  $(\hat{G}^{-1})^{ij}$  has

the following form:

$$(G^{-1}(k))^{11} = \frac{1}{k^2} \frac{c_{11} - (c_{11} - c_{44})n_1^2 + \Delta(c_{11} + c_{12})n_2^2 n_3^2}{c_{44} D(n)} \quad (12)$$

$$(G^{-1}(k))^{12} = -\frac{1}{k^2} \frac{(c_{12} + c_{44})(1 + \Delta n_3^2)n_1 n_2}{c_{44} D(n)}$$

$$\text{where } D(n) = c_{11} + \Delta(c_{11} + c_{12})(n_1^2 n_2^2 + n_1^2 n_3^2 + n_2^2 n_3^2) + \Delta^2 (c_{11} + 2c_{12} + c_{44})n_1^2 n_2^2 n_3^2;$$

$$n = k/k, \quad \Delta = \frac{c_{11} - c_{12} - 2c_{44}}{c_{44}}$$

The other components of the tensor  $G^{-1}(k)^{ij}$  are obtained by cyclic permutation of the Cartesian indices.

The elastic energy is given as:

$$E_1 = -\frac{(\theta_0 + \tilde{\theta}_0)^2}{2 D(n)} \left[ \gamma + n_1^2 A - n_1^4 B + \Delta C n_1^2 n_2^2 n_3^2 + 2\Delta \gamma^2 n_2^2 n_3^2 \right] \quad (13)$$

where:

$$\gamma = \frac{\epsilon_0 - \frac{\tilde{\epsilon}_0}{2}}{\epsilon_0 + \tilde{\epsilon}_0}$$

$$A = \frac{c_{11}}{c_{44}} + \left( \frac{c_{11}}{c_{44}} - 2 \right) \gamma^2 - 2\gamma \left( \frac{c_{12}}{c_{44}} + 1 \right)$$

$$B = \frac{c_{11}}{c_{44}} - 1 + \gamma^2 \left( \frac{c_{11}}{c_{44}} - 1 \right) - 2\gamma \left( \frac{c_{12}}{c_{44}} + 1 \right)$$

$$C = \frac{c_{11}}{c_{44}} + \frac{c_{12}}{c_{44}} + 2\gamma^2 \left( \frac{c_{12}}{c_{44}} - 1 \right)$$

From Eq. 13 it follows that the elastic energy of the crystal takes on its least value when the normal to the new-phase plate,  $n=k_0/k_0$ , is oriented in such a way that the right-hand side of Eq. 13 is at a minimum.

On analyzing Eq. 13 it can be shown that, depending on the relationship between the elastic constants  $c_{1j}$  and the value of the numerical factor  $\gamma$ , the energy is a minimum when the vector  $n$  lies either in the plane (100), or in (110). This means that the Miller indices of the plane of the crystal form (the plane of the plate) may either have the form (h0l) or (hhl).

To find the invariant plane (the orientational relationship) it is necessary to find the direction of the axis of rotation. For this we must know the direction of the vector  $\hat{G}^{-1} \hat{\sigma}_0 k_0$ . As the tensor  $\hat{\sigma}_{ij}^0$  has tetragonal symmetry, then both the vectors  $k_0$  and  $\hat{G}^{-1}(k_0) \hat{\sigma}_0 k_0$  lie either in the plane (100) or in (110). Since the vector  $\langle \gamma \rangle$  is the vector product of the vectors  $k_0$  and  $\hat{G}^{-1}(k_0) \hat{\sigma}_0 k_0$ , then the axis of rotation lies perpendicular to these planes. Thus when tetragonal deformations are present the invariant planes are either (100) or (110). All the results derived above are valid while it is possible to neglect the contribution made by surface tension. The effect of surface tension will be to prevent the "expansion" of the new-phase particle into an infinitely thin, infinitely wide plate.

In the general case the shape of the inclusion will be determined by competition between the elastic deformation energy, which is minimal for an inclusion in the form of an infinitely thin, infinitely wide plate, and the surface tension energy, which conversely, is minimal for an inclusion of equiaxial form.

Recent X-ray and microscopic studies show that in a number of cubic solid solution the periodical distribution of coherent inclusions of the cubic phase arise at an early stage of composition. This phenomenon was observed in Cu-Ni-Co<sup>2,3</sup>, Cu-Ni-Fe<sup>1,4</sup>, Cu-Be<sup>5,6</sup>, in a group of nickel-based alloys<sup>7,8,9,10</sup>, Au-Pt<sup>11</sup>, Fe-Be<sup>12</sup>,

Co-Pt<sup>13</sup>. This observation has investigated theoretical work on the elastic interaction between individual inclusions<sup>14,15</sup>.

Eshelby<sup>14</sup> has shown that there is no interaction among centres of dilatation in an elastically isotropic medium. Sometimes particles of a separated phase have an "equiaxed" form which is nearly spherical. In ref. 9, the interaction potential of two spherical inclusions was calculated under the assumption that the interaction is due to the differences in elastic moduli of the inclusions and matrices, and that the tensor  $\epsilon_{ij}^0$  described a pure dilatation. In this case the potential goes as  $1/r^6$  and decreases rapidly.

However, defects or precipitates which give rise to tetragonal distortions can interact quite strongly. The presence of a strong interaction must lead to correlations in the relative positions of the inclusions (short-range and possibly long-range order) during their formation in the field of already formed inclusions and also in their subsequent growth.

In the theoretical work of the elastic interaction of tetragonal distorted spheres Khachaturyan and Shatalov<sup>15</sup> have showed that the existence of strain field which differ from purely dilatation fields, leads to a complicated angular dependence in the potential even for the isotropic continuum model. Following ref. 15, if the

elastic moduli of both phases are equal the elastic energy of the medium with the inclusions of the new phase, relative to the undeformed state, is:

$$E_{el} = \sum_{p=1}^z \int (\hat{\mathcal{G}}_{ij}^0(p) \mathcal{E}_{ij}(r) \Theta_p(r) + \frac{1}{2} \lambda_{ijklm} \mathcal{E}_{ij}(r) \mathcal{E}_{lm}(r)) d^3r \quad (14)$$

where:  $\hat{\mathcal{G}}_{ij}^0(p) = \lambda_{ijklm} \mathcal{E}_{lm}^0(p)$ ;  $\lambda_{ijklm}$  is the elastic moduli tensor;  $\mathcal{E}_{ij}(r)$  is the strain tensor;  $\tilde{\Theta}_p(r)$  a function which is one inside the inclusion  $p$  and zero outside it;  $z$  is the number of inclusion types. Transforming to Fourier components Eq. 14 becomes:

$$E_{el} = -\frac{1}{2} \sum_{p,q} \int (n, \hat{\mathcal{G}}^0(p) G(n) \hat{\mathcal{G}}^0(p) n) \Theta_p(k) \Theta_q^+(k) \frac{d^3 k}{(2\pi)^3} \quad (15)$$

where  $k$  is the wave vector of the Fourier transformation;  $n = k/k$ ; the symbol  $(\dots, \dots)$  indicates the scalar product;  $\hat{\mathcal{G}}^0(p)$  and  $G(k)$  are operators whose matrix elements are  $\hat{\mathcal{G}}_{ij}^0(p)$  and  $G_{ij}(k)$ , where  $G_{ij}(k)$  is the Fourier component of the Green's tensor for the elastic problem.

The function  $\Theta_p(k)$  can be multiply connected. For simplicity it will be considered a medium in which there are only two inclusions altogether. Then, if the origin is put at the center of mass of one inclusion at

type  $p$  designating the form factor of this simply connected inclusion by  $\Theta_p(k)$ , the form factor of the other simply connected inclusion of type  $q$ , located at a distance  $r$  from the origin, has the form  $\Theta_q(k)e^{ikr}$ , where  $\Theta_q(k)$  is calculated in a coordinate system with origin at  $r$ .

It follows from Eq. 15 that the interaction of these two inclusions is given by the expression:

$$E_{in}^{pq} = -\frac{1}{2} \int A_{pq}(n) \Theta_p(k) \Theta_q^+(k) e^{-ikr} \frac{d^3 k}{(2\pi)^3} \quad (16)$$

where:  $A_{pq}(n) = \langle n, \hat{\sigma}^0(p)G(n) \hat{\sigma}^0(q)n \rangle$ . The quantity  $A_{pq}(n) \Theta_p(k) \Theta_q^+(k)$  is the Fourier component of the pair-interaction potential.

Using the isotropic continuum model to solve  $A_{pq}(n)$ , the interaction of two inclusions is given by the expression:

$$E_{in}^{pq} = \frac{V_1 V_2}{16} \left[ \frac{2 D_2^{pq}}{r^3} + \frac{(R_1^2 + R_2^2) D_4^{pq}}{5 r^5} \right] \quad (17)$$

where  $D_2^{pq}$  and  $D_4^{pq}$  are complicated terms depending on the orientation of the particles relative to the radius

vector which connects the two particles. The first term in Eq. 17 is the interaction for distances much greater than the inclusion dimension, and the second term is connected with the inhomogeneity of the deformation field of one inclusion at the limits of the region occupied by the other inclusion.

The expressions for the total energy of the elastic stresses of the system of coherent inclusion may be written in the general form:

$$E = E_0 + E_{int} \quad (18)$$

The first term in Eq. 18 does not depend on the mutual arrangement of the inclusions, it is the sum of the elastic self-energies of inclusions. The second term in Eq. 18, on the contrary, depends on the spatial distribution of the inclusions. Consequently it represents the stress-induced interaction energy of the inclusions, caused by the interference of the stress fields associated with each inclusion. One of the most interesting aspects of the potential in Eq. 18 is that it can have the form of a potential with a minimum;  $\partial E_{int} / \partial r = 0$ . It has been shown that the resulting potentials can be monotonically attractive, monotonically repulsive, or can have a minimum at a specific value of the interparticle spacing.

Since  $E_{int} \sim V_1 V_2$ ,  $E_{int}$  is maximal when



$V_1 = V_2$ , other conditions being equal. This means that the inclusions "try" to have the same dimensions if  $E_{int}$  is negative, for then  $E_{int}$  is minimal. Thus, the elastic interaction appears as a factor which stabilizes the dimensions of the particles if this interaction is attractive.

The theoretical treatment has been extended to multiparticle arrays<sup>16</sup>. It was shown that three types of periodic arrays are possible: a one-dimensional system of parallel lamellae; a two-dimensional distribution which may be viewed as a planar square macro-lattice formed by rods of the second phase; a three-dimensional primitive cubic macro-lattice which is equivalent to the macro CsCl.

The cause of all modulated structures, including those produced by spinodal decomposition, is the minimization of strain energy of the array. All modulated or tweed structures thus far observed can be referred to one of these general types. Their development in an ordinary precipitating system will begin with randomly distributed supercritical nuclei which produce increasing displacements as they grow (and coarsen) until the stresses become sufficiently high such that they affect the diffusional processes. These will then become anisotropic in such a way as to favour the growth of periodic arrays whose elastic energy is minimum - completely analogous

to those produced by spinodal decomposition when  $\delta$  is significant<sup>17</sup>.

Thus, coherent precipitation associated with coherency strains and higher volume fractions of precipitates will always result in quasi-periodic wave-like arrays of matrix and particles which are extremely similar to spinodally decomposed structures with composition-waves.

It can be seen that spinodal decomposition cannot simply be distinguished by the resulting microstructure: the origin of periodically modulated, coherent arrays is a minimization of elastic strain energy by anisotropically stress-affected diffusion in all cases.

## II. 2. Elastic stabilization of arrays of precipitates against Ostwald ripening

Recently it has become clear that the theory of Lifshitz<sup>18</sup> and Wagner<sup>19</sup> derived for a liquid matrix can be applied to describe the growth of certain coherent precipitates. The theory predicts that, when the rate of coarsening is controlled by the diffusion of the solute species through the matrix, the variation of the mean radius,  $\bar{r}$ , with time,  $t$ , of a dispersion of spherical particles is given by:

$$\bar{r}^3 - \bar{r}_0^3 = \frac{8 \gamma D C_0 v_m^2}{9 R T} (t - t_0) \quad (19)$$

where  $\bar{r}$  is the mean particle radius when coarsening commences at  $t = t_0$ ,  $\gamma$  is the specific precipitate-matrix interfacial free energy,  $D$  and  $C_0$  are the diffusivity and equilibrium molar concentration, respectively, of the solute species in the matrix phase at the temperature  $T$ ,  $V_m$  is the molar volume of the precipitate and  $RT$  has its usual meaning.

The experiments have indicated that only in the very special case of misfit-free alloys can the spheres of Lifshitz-Wagner size distribution be expected.

In alloys with a certain misfit between  $\gamma$  and  $\gamma'$ , the precipitates again are spheres which grow according to Lifshitz-Wagner law at the beginning of precipitation. However, at a some size, they start to change shape and local distribution.

In ref. 9 and 10, they found that the occurrence of this deviation from spherical shape and of the anisotropic local distributions is only a function of misfit between  $\gamma$  and  $\gamma'$ .

Boyd and Nicholson<sup>20</sup> have measured coarsening rates and particle-size distribution, in Al-Cu alloys, using the Lifshitz-Wagner theory, modified for the case of disc-shape particles. They have found that the coarsening behaviour of  $\theta''$  agrees quantitatively and qualitatively with the theory, but the coarsening behaviour of  $\theta'$  is anomalous (Fig. 1).

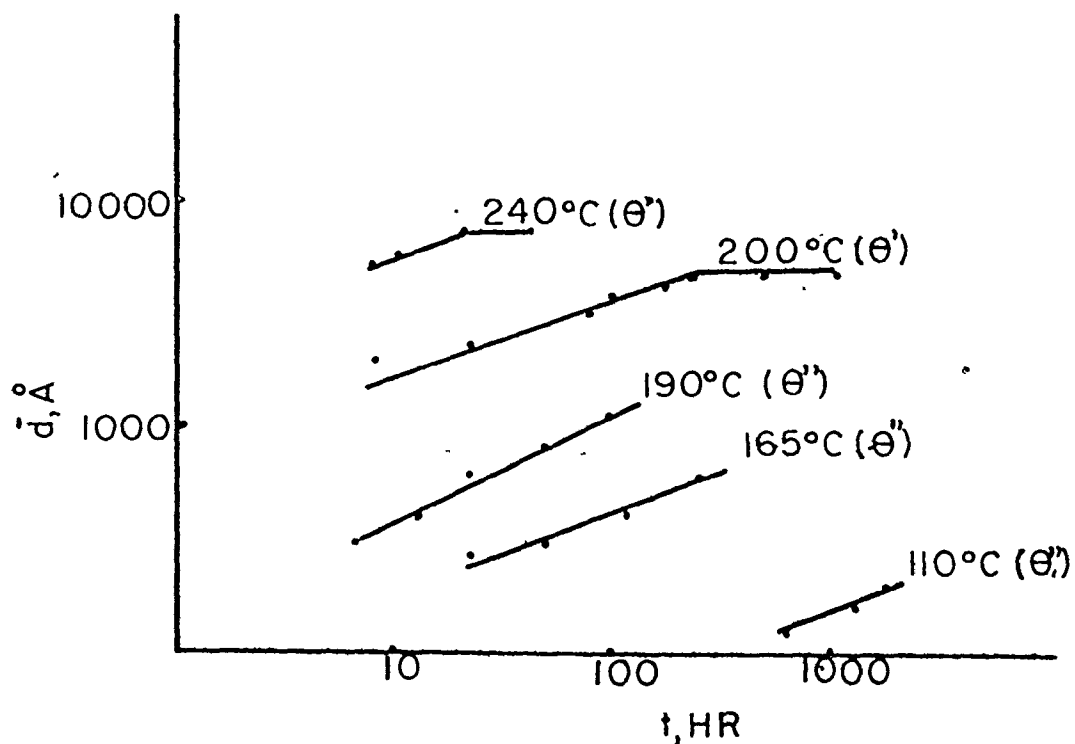


FIG. 1

Ham et al<sup>21</sup> reported on the solidification, ageing behaviour and creep properties of the inter-metallic compound  $\text{Ni}_3(\text{Al}, \text{Ti})$ , strengthened by a bimodal distribution of  $\gamma$  precipitates. They have found, when these alloys are solidified rapidly under planar interface conditions to give a uniformly supersaturated parent phase, and then aged, that no correlation of  $\gamma$  platelet length with ageing time exists for the resulting unimodal dispersion of platelets. They have presumed that the platelets give rise to tetragonal distortion and that the array is stabilized by elastic interaction.

It was shown that the elastic energy tends to stabilize equal sized precipitates ( $E_{\text{int}} \sim V_1 V_2$ ,  $E_{\text{int}}$  is maximal when  $V_1 = V_2$ ), whereas the surface energy has a maximum for  $V_1 = V_2$ , and a certain range of fluctuation in volume will relax to the equal volume state. The equilibrium is metastable, because  $E_{\text{surface}}$  has infinite slopes for  $V_1 = 0$  and for  $V_2 = 0$ ; thus, a large enough fluctuation will cause one precipitate to grow at the expense of the other.

Thus certain types of elastic interaction can stabilize two precipitates against competitive growth, and it is reasonable to suppose that elastic interaction can stabilize an array of precipitates against Ostwald ripening.

### II. 3. Previous work on Al - 4% Cu

The precipitation processes in aluminium-copper have been studied by a variety of techniques over the past fifty years. The extensive X-ray investigations have been reviewed by Hardy and Heal<sup>22</sup>. The more recent electron microscopy and electrical resistivity observations have been discussed by Kelly and Nicholson<sup>23</sup>.

These investigations have demonstrated the existence of several metastable precipitate phases in addition to the equilibrium  $\text{CuAl}_2$  ( $\Theta$ ) phase. The precipitation sequence for a aluminium - 4% copper

alloy aged below 175°C is:

G. P. zones  $\rightarrow \Theta'' \rightarrow \Theta' \rightarrow \Theta$

Using X-ray techniques, Guinier<sup>24</sup>, Preston<sup>25</sup> and Gerold<sup>26</sup> deduced that G.P. zones are thin copper rich platelets, probably one or two/atom planes thick, lying on  $\{100\}$  planes of the aluminium matrix. Both  $\Theta''$  and  $\Theta'$  are ordered arrangements of copper and aluminium atoms with tetragonal unit cells. The precipitates are thin discs with the  $c$  axis perpendicular to the habit plane, and the orientational relationship is:

$$\{100\} \Theta'' , \Theta' \parallel \{100\}_\alpha$$

The structure of  $\Theta''$ , as determined by Guinier is shown in Fig. 2:

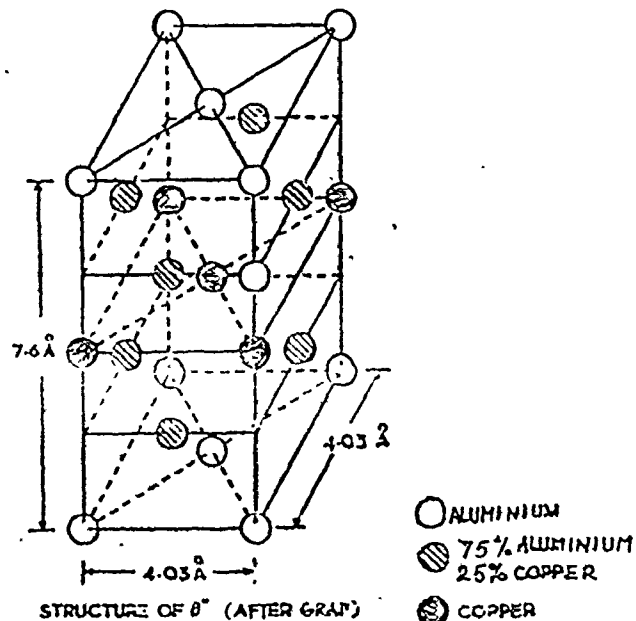


FIG. 2

Silcock et al<sup>27</sup> have pointed out that when  $\Theta''$  forms from G.P. zones, the  $c$  parameter changes from 8.0 to 7.6 Å as the  $\Theta''$  precipitates grow. Because the maximum misfit between the  $\Theta''$  and matrix lattice planes is about 5 percent,  $\Theta''$  is coherent across all interfaces. The misfit in the  $c$  direction is taken up by elastic displacements in the matrix, as shown in Fig. 3:

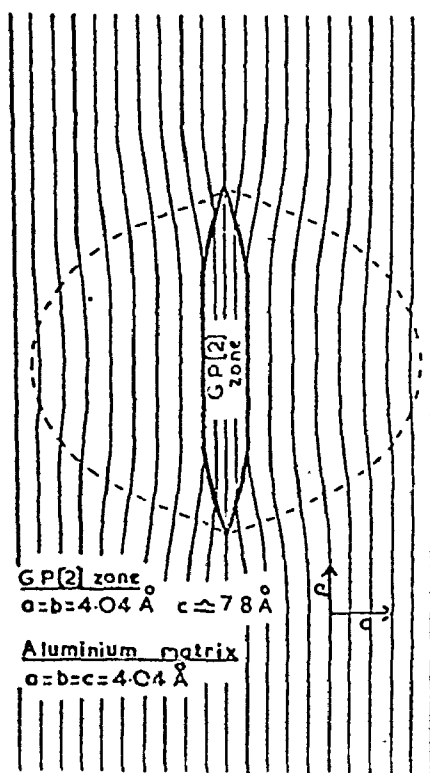


FIG. 3

The structure of  $\Theta'$ , as determined by Silcock et al is shown in Fig. 4.  $\Theta'$  is coherent across the interface parallel to the habit plane, but owing to the large misfit in the  $c$  direction, it is non-coherent across the interface at the periphery of the disc.

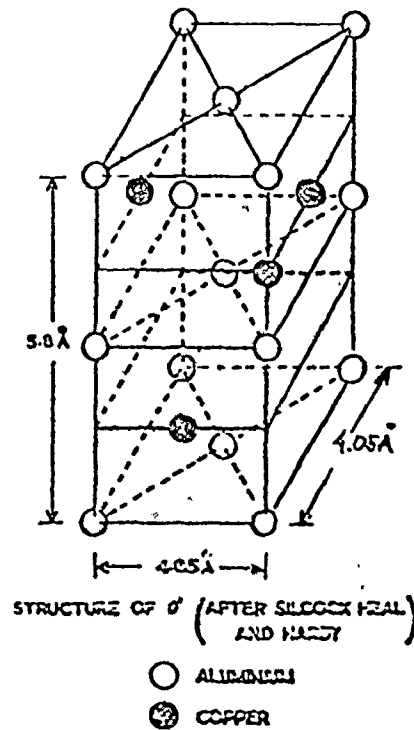


FIG. 4

$\Theta$  is tetragonal with  $a = 5.066 \text{ \AA}$  and  $c = 4.374 \text{ \AA}$ . For ageing temperatures below  $300^\circ\text{C}$  occurs in the grain boundaries only.



## II. 4. An approximation for the strain field of a disc-shaped

### G.P. zone

Several models have been proposed for the strain field of disc-shaped zones. Guinier<sup>28</sup> based his model on the Fourier transform of intensity distributions observed from low-angle diffuse X-ray scattering, while others<sup>29,30</sup> calculated intensities from assumed strain fields, and compared these with intensities observed in diffuse X-ray scattering experiments.

Nabarro<sup>31</sup> had noted that a collapsed disc of vacancies may be regarded essentially as a prismatic dislocation loop. Franz and Kroner<sup>32</sup> showed that a disc-shaped precipitate such as a G.P. zone in which the size-factor was negative (Al-Cu, Cu-Be, Au-Ni) could also be treated as a prismatic loop having a Burgers vector equal in magnitude to the difference in size of the solute and solvent atoms. The calculation of finite prismatic loops has been carried out in detail by Bullough and Newman<sup>33</sup> and Kroupa<sup>34</sup>.

When the diameter of the loop is small compared to the detail required, it is possible to treat a prismatic loop as a point singularity in an elastic continuum<sup>35</sup>. Kroupa specialized the derivation used by Eshelby<sup>14</sup> for the more general case of an ellipsoidal inclusion. Following Kroupa<sup>35</sup>, the displacement at a large distance

from the particle, i.e. at a distance much larger than the dimensions of the particle is:

$$du_i = \frac{k_0}{r^2} \left\{ \frac{1-2\nu}{r} \left[ n_l b_k r_k + b_i n_k r_k - r_i b_k n_k \right] + \frac{3r_i b_k r_k n_l r_l}{r^3} \right\} dA \quad (20)$$

where  $k_0 = -\frac{1}{8\mu(1-\nu)}$

The stress tensor  $d\sigma_{ij}$  around an infinitesimal loop can be calculated from Eq. 20 using Hook's law:

$$\begin{aligned} d\sigma_{ij} = & \frac{2k_0\mu}{r^3} \left\{ \left[ \frac{3(1-2\nu)}{r^2} b_k r_k n_l r_l + (4\nu - 1)b_k n_k \right] \delta_{ij} + \right. \\ & + (1-2\nu)(b_i n_j + n_i b_j) + \frac{3\nu}{r^2} \left[ b_k r_k (n_i r_j + r_i n_j) + \right. \\ & \left. \left. + n_k r_k (b_i r_j + r_i b_j) \right] + \frac{3(1-2\nu)}{r^2} b_k n_k r_i r_j - \right. \\ & \left. - \frac{15}{r^4} b_k r_k n_l r_l r_i r_j \right\} dA \quad (21) \end{aligned}$$

It is apparent that the displacements decrease

with distance  $r$  as  $1/r^2$  and stresses as  $1/r^3$ .

Equations 20 and 21 can be simplified by using a special coordinate system, Fig. 5:

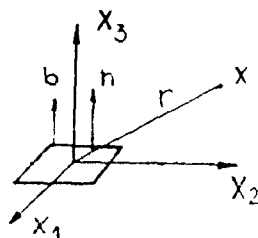


FIG. 5

The loop is at the origin of the coordinate system in the  $x_1x_2$  plane ( $n_1=n_2=0, n_3=1$ ) and separately introduces displacements and stresses for a pure prismatic infinitesimal dislocation loop ( $b_1=b_2=0, b_3=b$ ) which are:

$$\begin{aligned}
 u_1 &= \frac{k x_1}{6 r^3} \left[ - (1 - 2\nu) + \frac{3 x_3^2}{r^2} \right] \\
 u_2 &= \frac{k x_2}{6 r^3} \left[ - (1 - 2\nu) + \frac{3 x_3^2}{r^2} \right] \\
 u_3 &= \frac{k x_3}{6 r^3} \left[ 1 - 2\nu + \frac{3 x_3^2}{r^2} \right]
 \end{aligned} \tag{22}$$

$$\sigma_{11} = \frac{kM}{r^3} \left[ \frac{4\nu - 1}{3} + (1 - 2\nu) \frac{x_1^2 + x_3^2}{r^2} - \frac{5 x_1^2 x_3^2}{r^4} \right]$$

$$\sigma_{22} = \frac{kM}{r^3} \left[ \frac{4\nu - 1}{3} + (1 - 2\nu) \frac{x_2^2 + x_3^2}{r^2} - \frac{5 x_2^2 x_3^2}{r^4} \right]$$

$$\sigma_{33} = \frac{kM}{r^3} \left[ \frac{1}{3} + \frac{2 x_3^2}{r^2} - \frac{5 x_3^4}{r^4} \right]$$

(22)

$$\sigma_{12} = kM \frac{x_1 x_2}{r^5} \left[ 1 - 2\nu - \frac{5 x_3^2}{r^2} \right]$$

$$\sigma_{13} = kM \frac{x_1 x_3}{r^5} \left[ 1 - 5 \frac{x_3^2}{r^2} \right]$$

$$\sigma_{23} = kM \frac{x_2 x_3}{r^5} \left[ 1 - 5 \frac{x_3^2}{r^2} \right]$$

where:  $k = - \frac{3 b_3}{4\sqrt{1-\nu}} dA,$

$b$  = Burgers vector,

$dA$  = area of the loop,

$$r^2 = x_1^2 + x_2^2 + x_3^2,$$

$M$  = shear modulus,

$\nu$  = Poisson ratio assumed = 1/3

## II. 5. Interaction between pairs of dislocation loops

### - the infinitesimal approximation -

The total energy of a pair of dislocation loops is simply the self energy of each loop plus the interaction energy between the two. This interaction energy is defined as the energy required to create one loop in the stress field of another.

For the general case using Kroupa's notation:

$$E_{\text{int}} = n_i^{(2)} \mathcal{G}_{ii}^{(1)} b_i^{(2)} \delta A^{(2)} \quad (23)$$

where:  $\mathcal{G}_{ii}^{(1)}$  is the stress tensor from loop 1 at loop 2,

$n_i^{(2)}$  - unit normal at loop 2,

$b_i^{(2)}$  - Burgers vector of loop 2,

$\delta A^{(2)}$  - area of loop 2

(subscripts follow the Einstein convention).

For a parallel prismatic dislocation loops (Fig. 6) Eq. 23 becomes:

$$E_{\text{int}} = - \pi a^2 \mathcal{G}_{33} b \quad (24)$$

where:  $a$  = loop diameter,

$\mathcal{G}_{33}$  = stress field of 1 at 2,

$b$  = Burgers vector of loop 2.

Substituting  $\sigma_{33}$  from Eq. 22 gives:

$$E_{\text{int}} = - \frac{\pi a^4 b^2 \mu}{8 R^3} \left[ 3 + \frac{18x_3^2}{R^2} - \frac{45x_3^4}{R^4} \right] \quad (25)$$

where:  $\mu$  = shear modulus,  
 $R^2 = x_1^2 + x_2^2 + x_3^2$

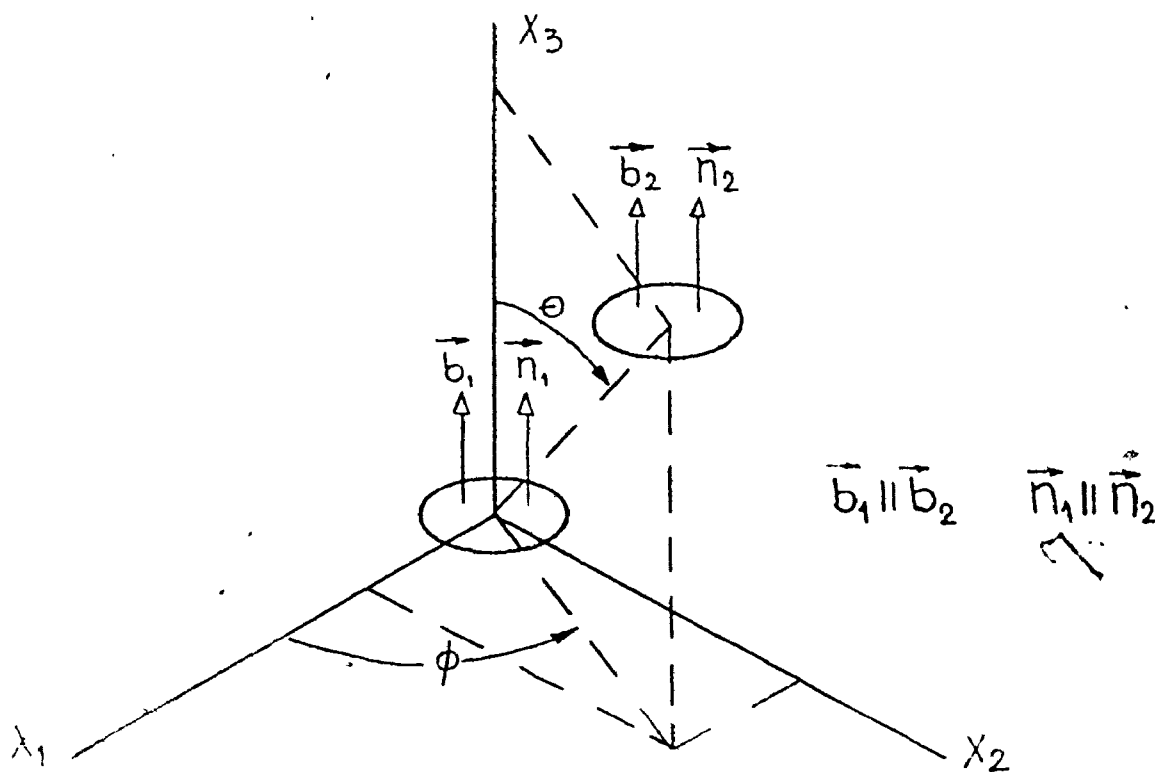


FIG. 6

Similarly for perpendicular prismatic loops  
(Fig. 7):

$$E_{int} = - \pi a^2 \dot{\phi}_{11} b \quad (26)$$

Substitution  $\dot{\phi}_{11}$  from Eq. 22 gives:

$$E_{int} = - \frac{\pi a^4 b^2 \mu}{8 R^3} \left[ 1 + \frac{3(x_1^2 + x_3^2)}{R^2} - \frac{45 x_1^2 x_3^2}{R^4} \right] \quad (27)$$

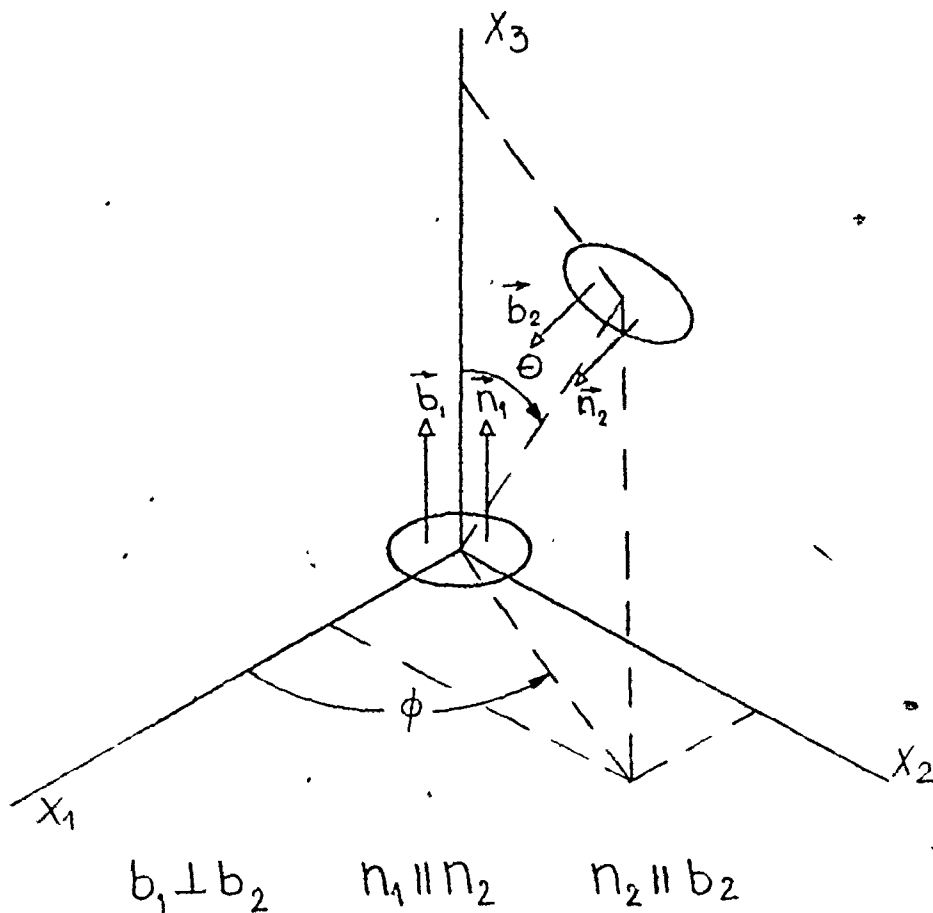


FIG. 7

Examples of this kind of interaction for various relative orientations of precipitates are given by Eurin et al<sup>36</sup>. It has been shown that, depending of the configuration, interaction can be strongly attractive, strongly repulsive and other configurations which are intermediate between these extremes. For example, the edge-face configuration is strongly attractive and the face-face configuration is strongly repulsive.

From these interaction energies (and derivative forces) one can proceed to larger number of loops in different configuration; a balance may be obtained between the repulsion of two parallel coaxial loops and a loop placed midway perpendicular to both, etc.

Fillingham et al<sup>37</sup> have also used the infinitesimal loop approximation to calculate several ordered arrays of disc shaped zones in order to describe "tweed" structures and the diffraction contrast they yield in the transmission electron microscope.



## CHAPTER III

### INTERACTIONS AMONG FINITE PRECIPITATES

Brown et al<sup>38</sup> and Khachaturyan and Shatalov<sup>15</sup> have shown that the elastic interaction among the precipitates causing tetragonal distortions, in finite precipitates is qualitatively distinguishable from that in the infinitesimal approximation.

In order to determine the interaction energies between two disc-shape precipitates more precisely, the following procedure has been performed. A plate, taken in approximation as one dislocation loop, was divided into one hundred small platelets. After calculating the interaction energies among all of the platelets (using the infinitesimal approximation) the sum of all these energies was taken giving the total interaction energy between two precipitates.

This kind of calculation of interaction energies gives qualitatively and quantitatively different results from that using the infinitesimal approximation. In addition, an approximation of square plate-like precipitate shape was assumed instead of equilibrated disc-shape  $\Theta$  precipitate. This is expected to influence to some extent the quantitative results but not qualitative results. A computer was used to calculate interaction energies of finite precipitates because of the large number of

summation of interaction energies involved; between two plates a sum of  $10^4$  interaction energies was required.

Before starting the calculation of the total elastic energy of an array, the following conditions were required:

1. The minimum distance from the central precipitate for which the infinitesimal approximation method may be used.

2. The distance between precipitates which gives the maximum interaction energy.

To find the first condition, the interaction energies between two plates when they are mutually parallel (face-face and edge-edge configuration) and when they are perpendicular (edge-face configuration and edge-edge configuration) were calculated. The distance between the plates after each calculating step was increased by an increment of  $1/10$  length of the plates. The interaction energies according to these four combinations are shown in Figs. 8,9,10 and 11. This is compared with the interaction of infinitesimal precipitates (broken lines). From Fig.8 it is clear that the interaction energy of two finite square plates in face-face configuration is much less positive (repulsive) than the interaction energy of two infinitesimal precipitates of the same configuration.

This stems from the interaction of the elements

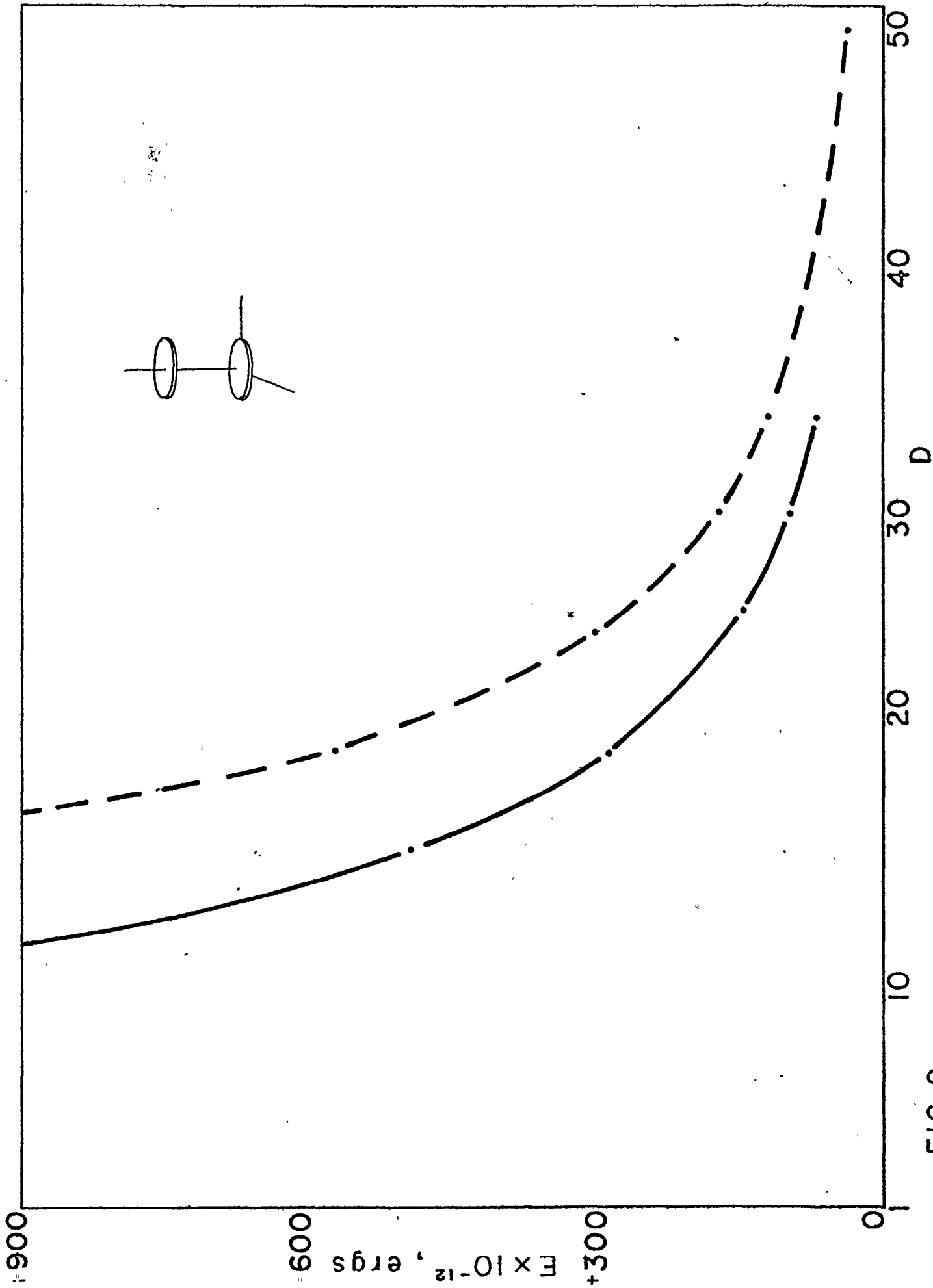


FIG. 8

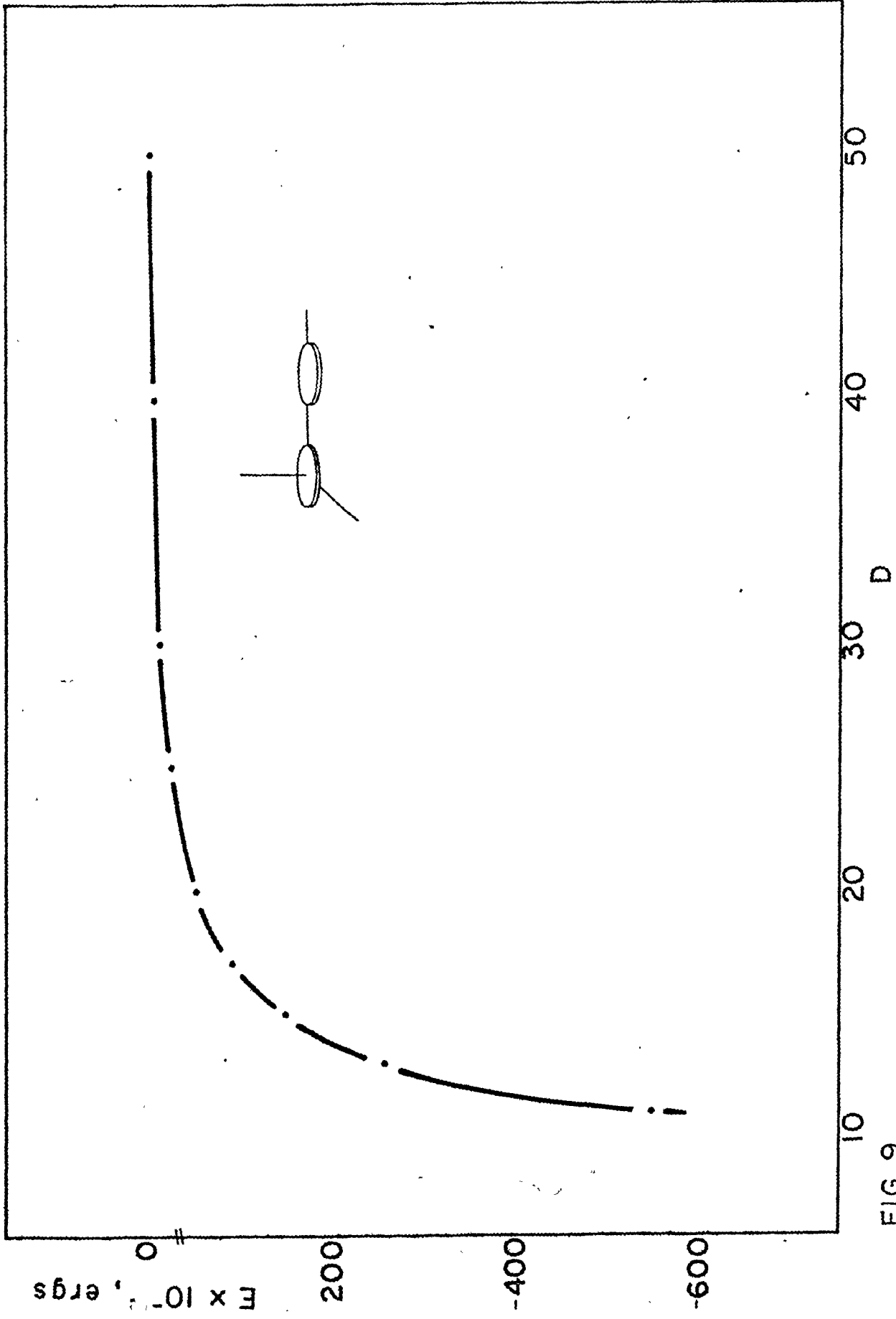


FIG. 9

Energy  $F \times 10^{-12}$  (ergs) versus distance  $D$ . The y-axis is inverted, with 0 at the top and -600 at the bottom. The x-axis ranges from 10 to 50. A dashed curve shows energy increasing from approximately -550 at  $D=10$  towards 0 as  $D$  increases. An inset diagram shows two ovals on a horizontal line, with a vertical line passing through the center of the left oval.

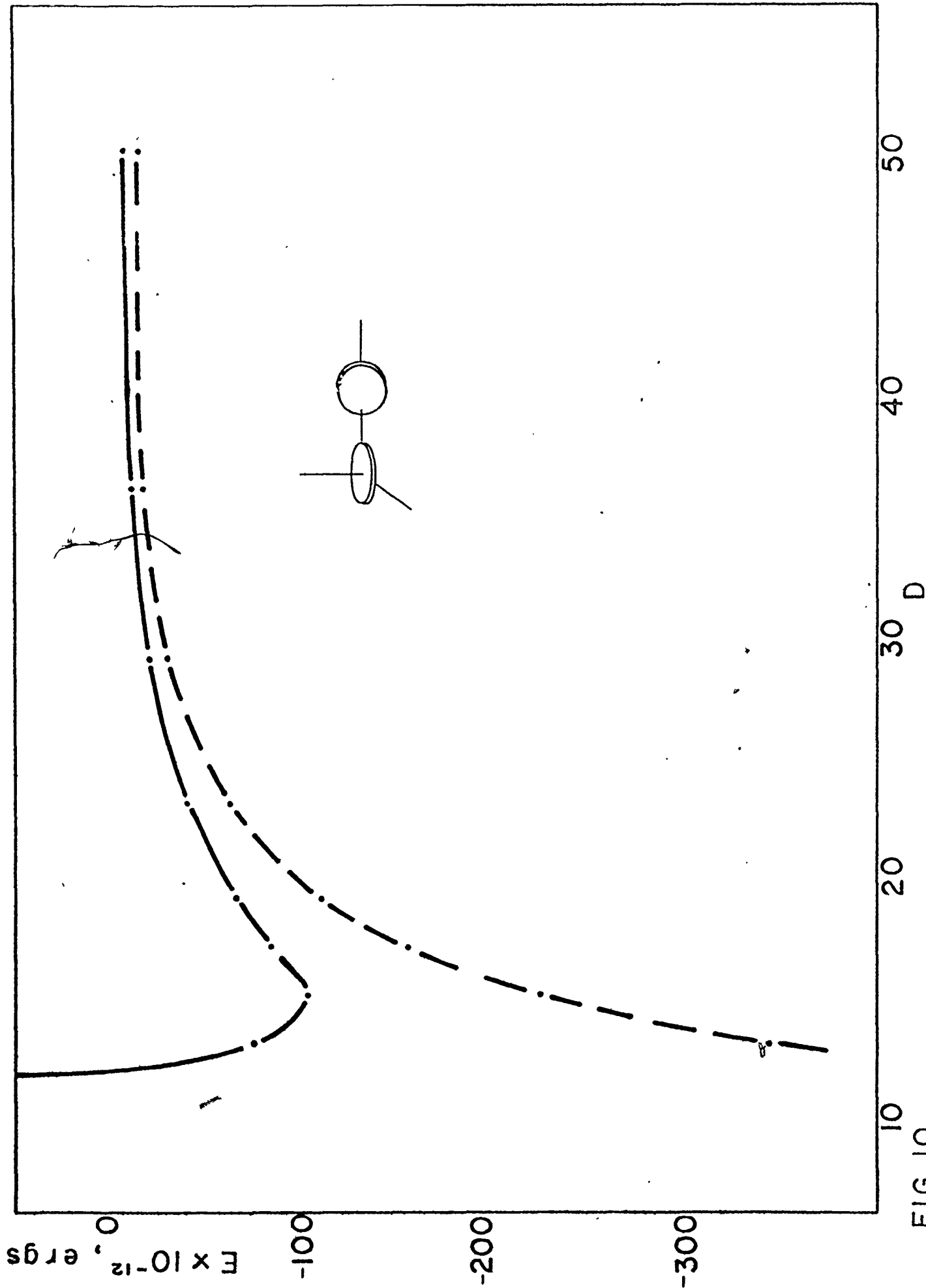


FIG.10

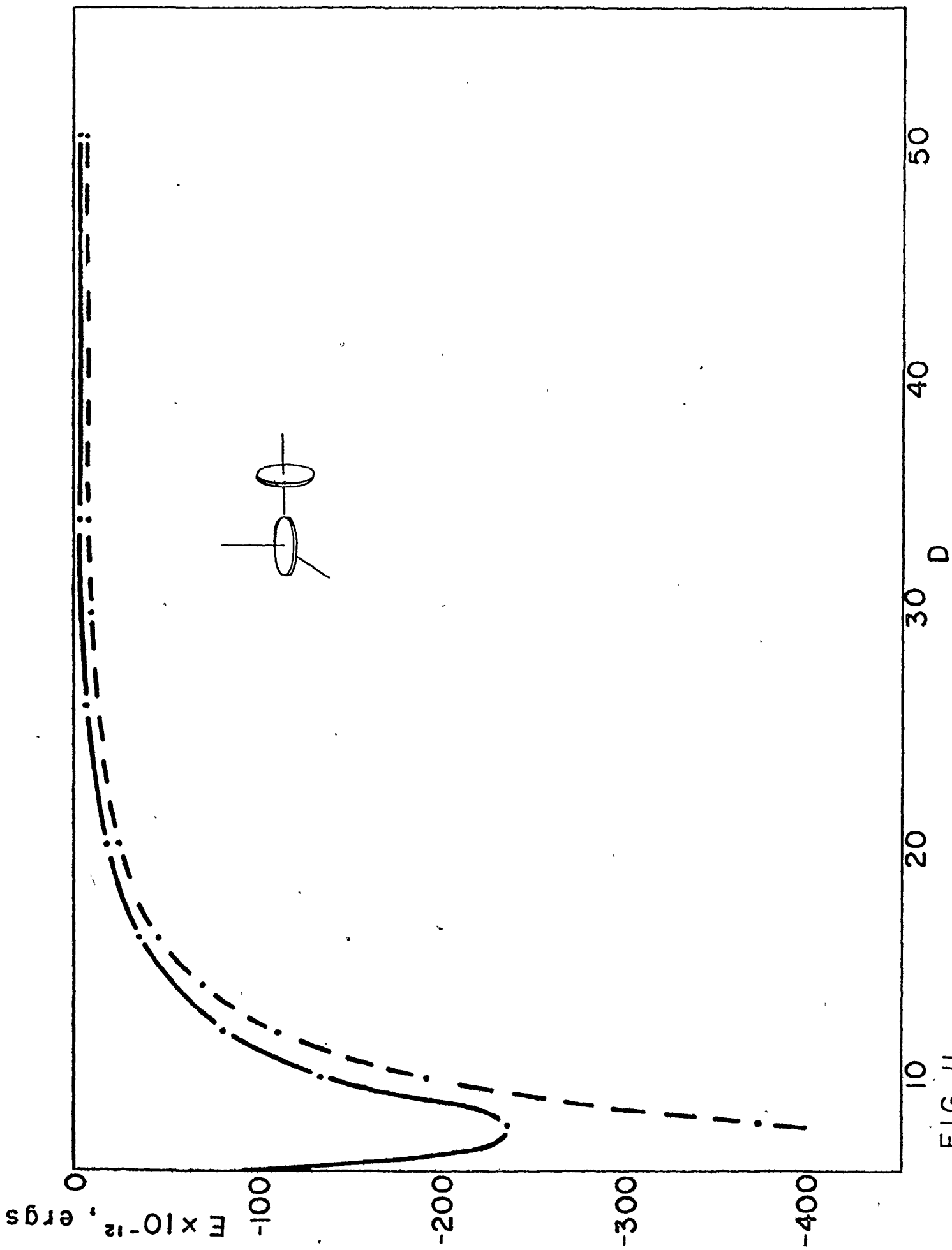


FIG. II

far away from the centres of the precipitates. More important, this interaction energy of elements far away from centres of the precipitates leads to the minimum in the interaction energy of two finite precipitates when they are mutually perpendicular in both combinations (as shown in Figs. 10 and 11). The appearance of the minimum on the interaction energies' curves gives a tridimensional stable configuration with respect to the displacement of the central plate, as will be shown later. A different result is obtained by using the infinitesimal approximation, where the displacement in same particular direction leads to mechanically unstable tridimensional configuration. This conclusion is in agreement with Figs. 10 and 11 where each displacement in the infinitesimal approximation leads the system to a lower energy state. According to the interaction energy curves (finite and infinitesimal) for all of these combinations a minimum distance of 50 units ( 5 times the edge length) from the central loop is considered a reasonable point at which to begin using the infinitesimal approximation in computing the interaction energies. Figs. 10 and 11 show that the minimum interaction energy appears at different distances from the central precipitate depending on mutual configuration. From these curves it is apparent that the tridimensional configuration may be obtained

by combining parallel (repulsive) and vertical (attractive) configurations in different ways.

Because, in general, a tridimensional array will be made up of parallel and perpendicular combinations, the separation of neighbouring plates corresponding to a minimum in energy, if such a minimum exists, will not be that given by Fig. 10 or by Fig. 11, but will be determined by some balance between attractive and repulsive configurations.

A Tyapkin array<sup>39</sup> was chosen for study (Fig.12). The energy as a function of precipitate separation (condition 2) was determined by calculating the total interaction energy for different distances between neighbouring precipitates.

The total energy of an array may be expressed as:

$$E_{\text{total}} = \sum_{i=1}^N E_{\text{self}} + \frac{1}{2} \sum_{i=1}^{N-1} \sum_{j=i+1}^N (E_{\text{int}})_{ij} \quad (28)$$

where  $E_{\text{self}}$  is the self energy of a loop,  $N$  is the total number of loops being considered,  $(E_{\text{int}})_{ij}$  is the interaction energy between the  $i$ -th and  $j$ -th loops. Since the self energy for (identical) loops, however



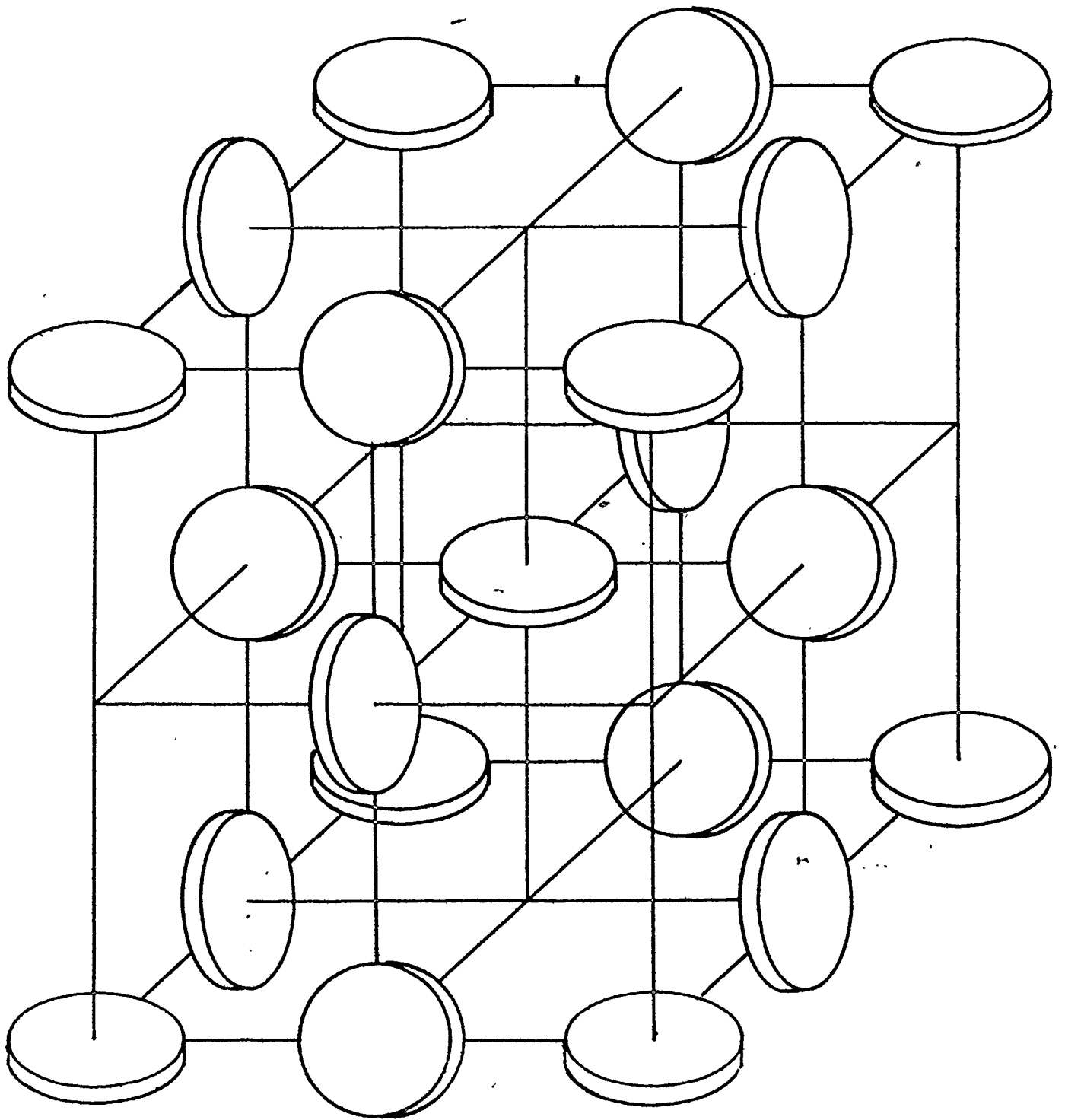


FIG. 12

TYAPKIN ARRAY

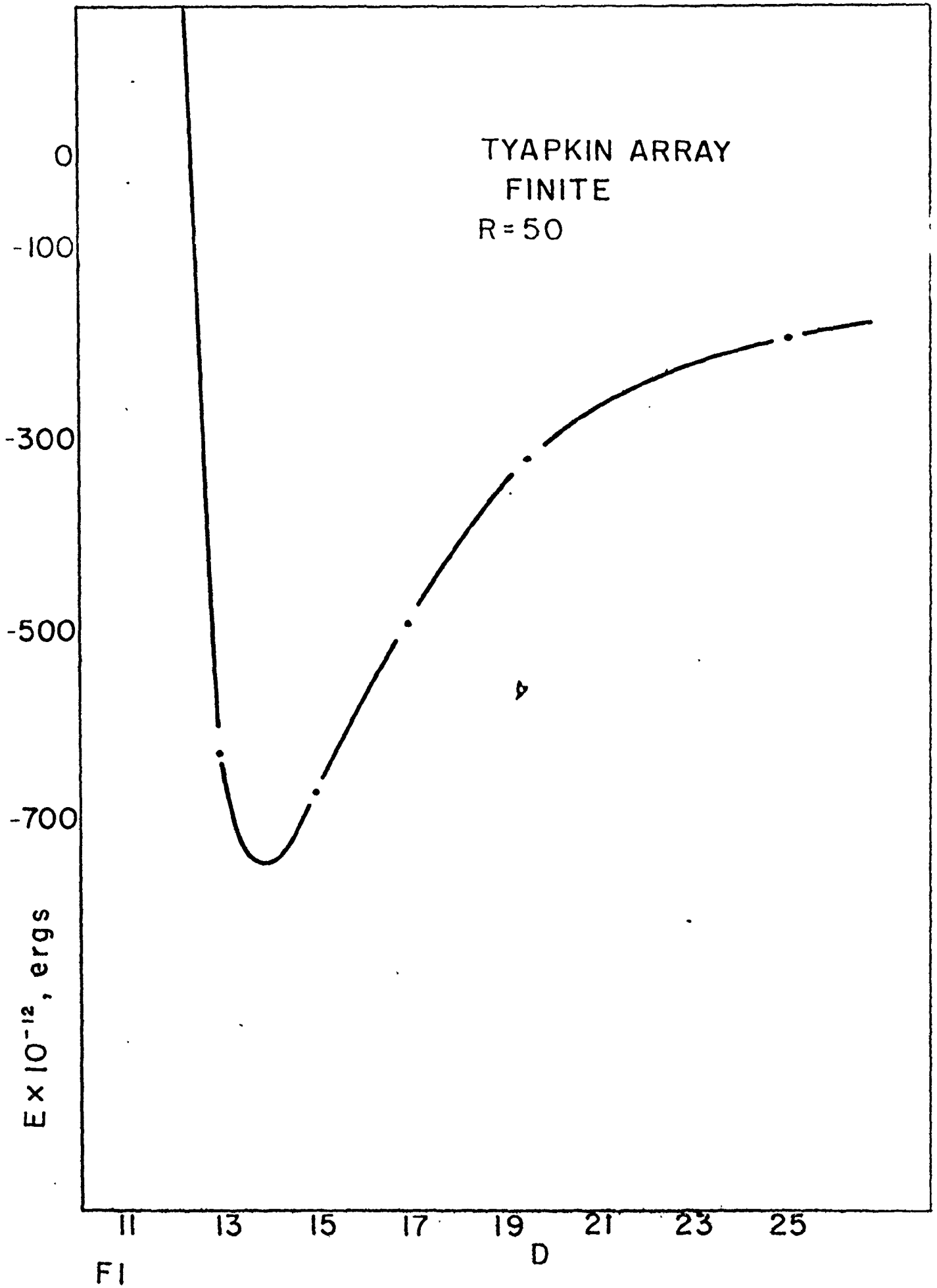
oriented, is constant for a given number of loops, this was neglected during computation. The interaction energies of precipitates lying in the limit of 50 units distance were computed using the finite approximation while the interaction energies of precipitates lying further away from the central precipitate were computed using the infinitesimal approximation.

The summation required care, since specific decisions were required (as the computation proceeded outward from a central loop) to determine the presence of a loop, and the distance between loops for which an interaction energy was being computed.

The total elastic energy per plate of the Tyapkin array versus the distance between the plates is shown in Fig. 13.

It is seen that there is a minimum on the energy curve (short range order) for a distance between neighbouring precipitates of about 15 units. This is determined e.g., by combinations of the potentials given in Figs. 8 - 11.

In order to estimate reliability of the approximation involved in treating precipitates more than 50 units from the central precipitate as infinitesimal, the corresponding calculation was performed for a cut-off radius of 100 units for interparticle separations near that for minimum energy (Fig. 14).



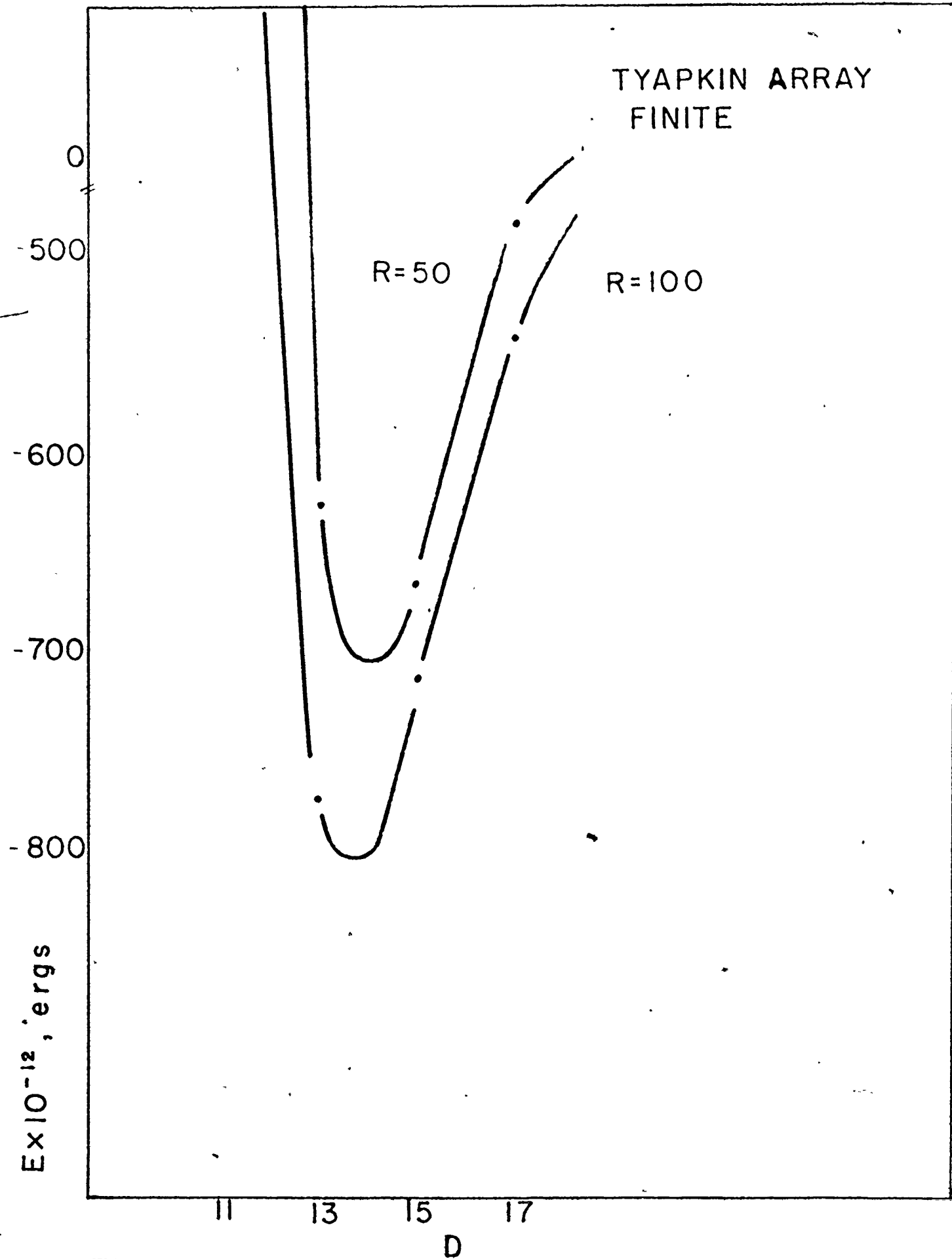


FIG.14

The Table I shows the total number of precipitates enclosed by spheres of radius 50 and 100 units, for near-neighbour separations of 13, 15 and 17 units.

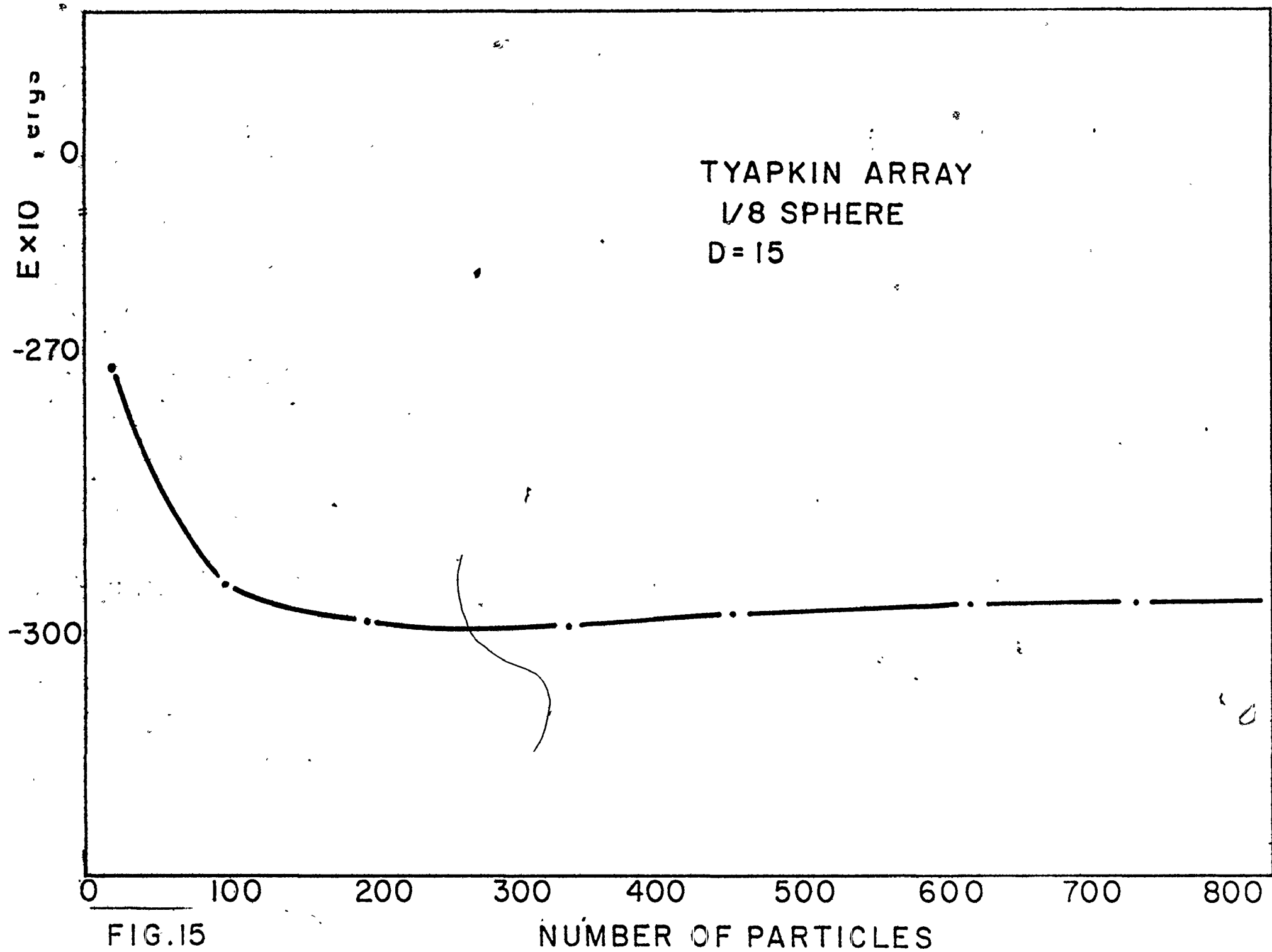
Table I

radius	number of particles		
	distance (centre to centre)		
	13	15	17
50	186	130	96
100	1450	902	622

By comparing the elastic energy curves of Fig. 14 is apparent that the energy difference is small and that the energy minimum occurs at the same separation for both curves.

The total elastic energy per plate of the Tyapkin array versus the number of precipitates is shown in Fig. 15.

As indicated on the diagram these energies were calculated for  $1/8$  of the sphere. Crudely, the total number of precipitates is  $\sim 8$  times greater. For example,



the point of 800 particles shown in Fig. 15 corresponds to the total number of about 5 to 6 thousand precipitates. Fig. 15 shows that the elastic energy reaches a minimum and that, on further addition of precipitates to the system, the energy starts to increase monotonically. It can be concluded that the greatest contribution to the elastic energy of the array comes from the nearest neighbours; this is in agreement with the potential decrease with  $1/r^3$  ( $\phi_{ij} \sim 1/r^3$ ).

In order to show the existence of a fundamental difference between the energy vs. separation curves for finite precipitates and those for infinitesimal precipitates the total elastic energy per plate of the Tyapkin array as a function of interparticle distance was calculated using the infinitesimal approximation (Fig. 16). It is obvious that this curve shows no minimum, and that it becomes increasingly more negative for smaller distances between the plates.

On the basis of this data it would appear that the Tyapkin array should be stable since it possesses a minimum in the interaction energy curve.

However, such a simple equilibrium criterion is incomplete. In order to be sure that the periodical distribution of inclusions is stable, it is necessary to study the changes of the interaction energy of precipitates with respect to their displacement from the

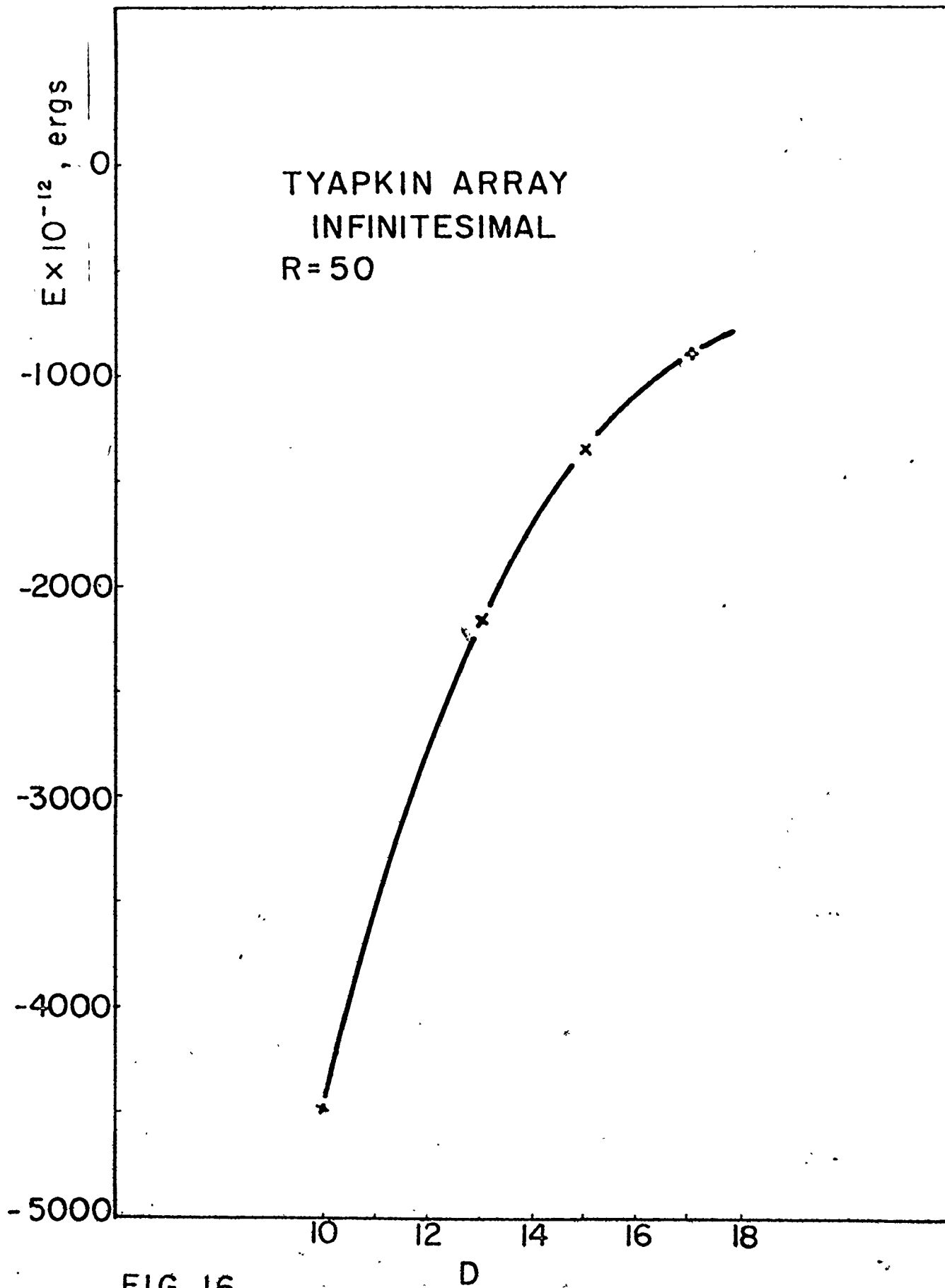
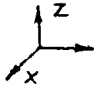


FIG. 16



position of the ideal lattice sites, and to the volume perturbations as well.

Therefore, the interaction energy calculations were made for the Tyapkin array but with the central plate's position altered a small amount, i.e. subjected to a virtual displacement along  $x$ ,  $y$  and  $z$  axes (the coordinate axes being disposed as shown schematically: ) and the total interaction energy calculated after each displacement. The results of the energies of finite precipitates are shown in Figs. 17 and 18.

The energy was calculated for the displacement in  $x$  and  $z$  directions. The displacement in  $y$  direction has not been taken into account due to symmetry. From Figs. 17 and 18 it is seen that the interaction energy increases by successive increment of the displacement along  $x(y)$  or  $z$  axes.

Consequently, the Tyapkin unit cell as a perfect array is also a mechanically stable configuration.

In addition, the Tyapkin array was tested for stability with respect to the displacement by applying the infinitesimal approximation as Fillingham et al<sup>37</sup> did. The results of these calculations are shown in Figs. 19 and 20. It can be seen that the array is mechanically stable only in the  $z$  direction, while it is unstable in the  $x$  and  $y$  directions because the energy decreases

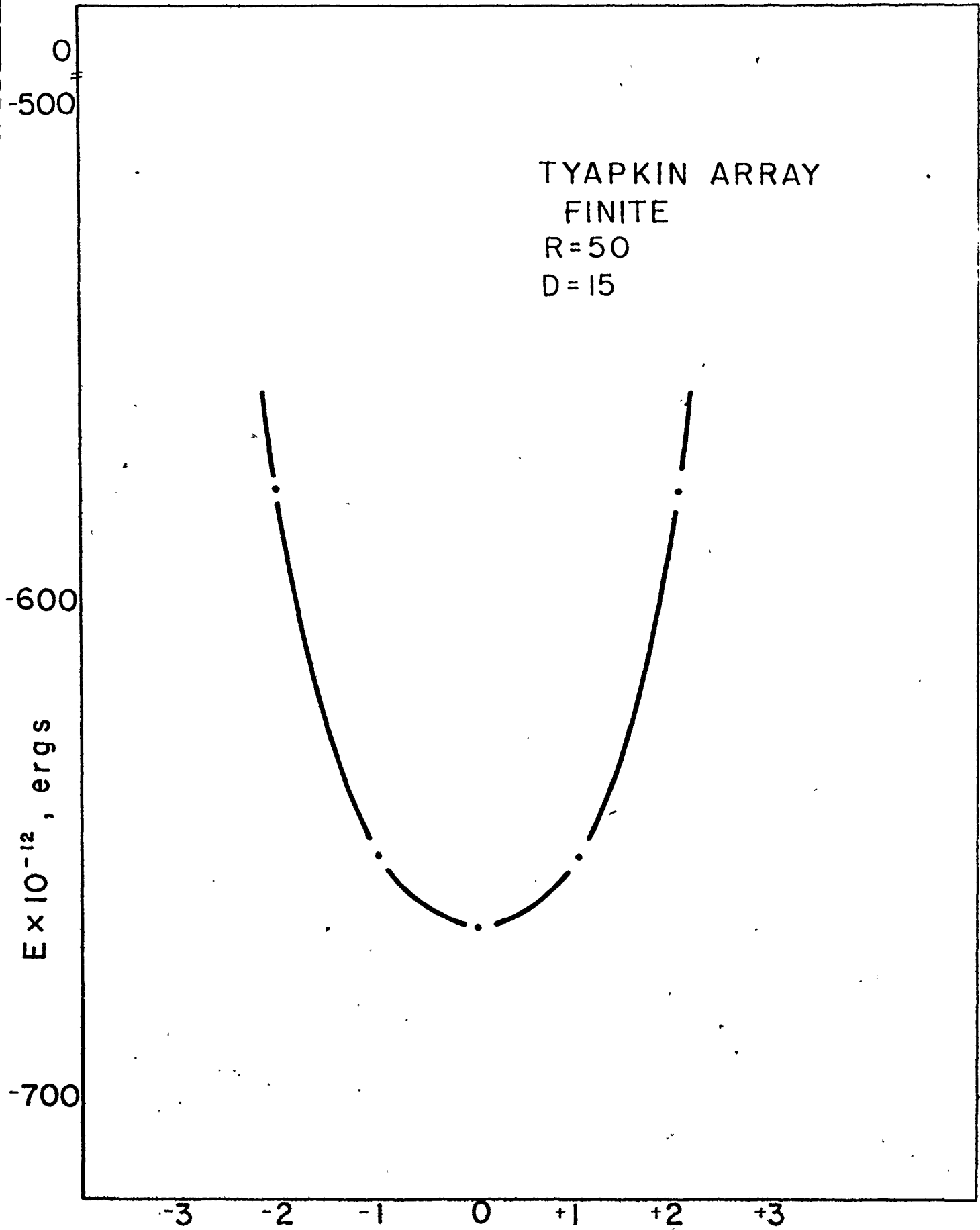
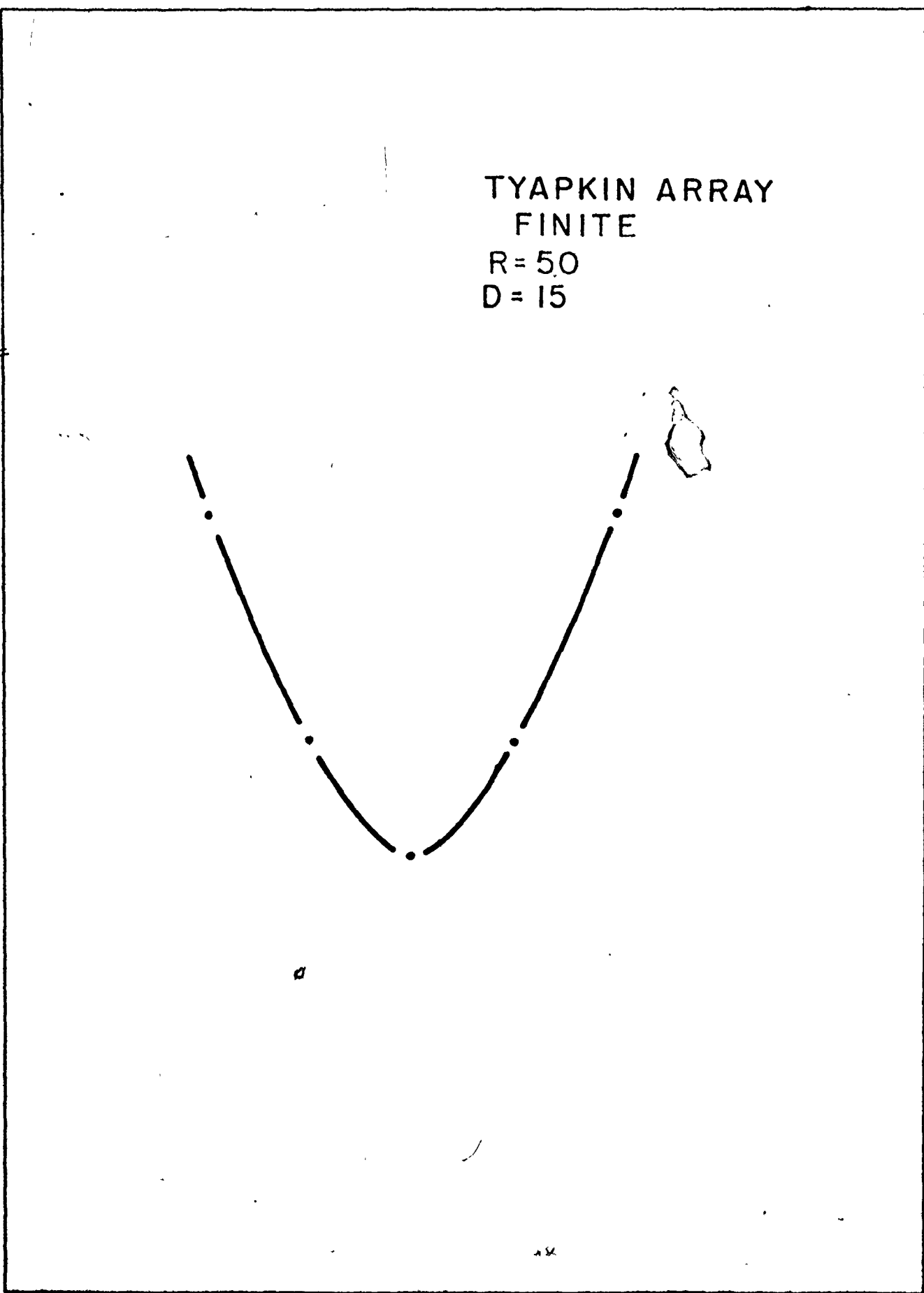


FIG.17 DISPLACEMENT OF CENTRAL PLATE,  $\Delta x$

TYAPKIN ARRAY  
FINITE  
R = 50  
D = 15

0  
600  
700  
E x 10<sup>-12</sup>, ergs



-3 -2 -1 0 -1 +2 +3  
IR T L TE

TYAPKIN ARRAY  
INFINITESIMAL  
R = 50  
D = 15

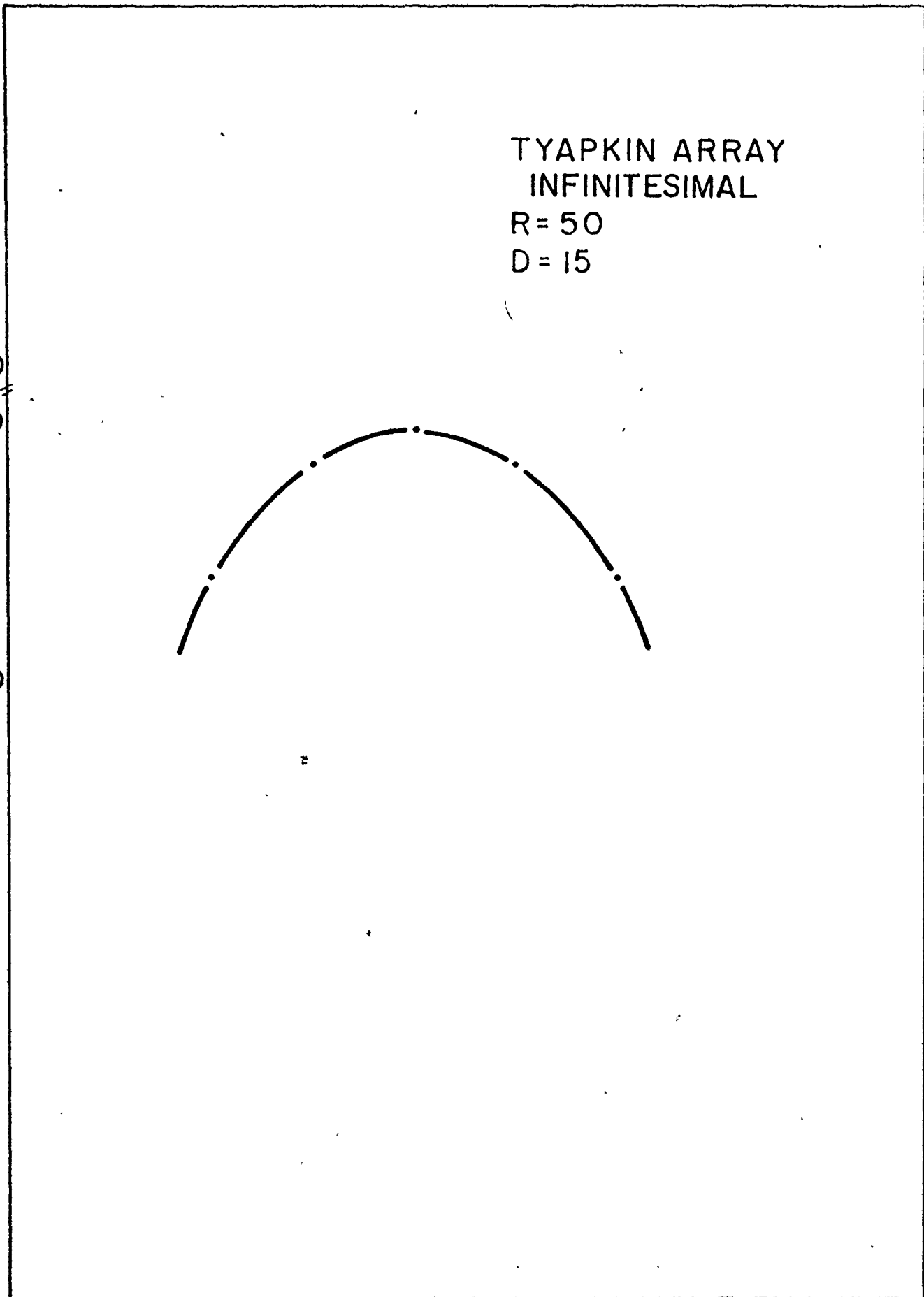
0  
-1350

-1000

$E \times 10^{-12}$ , ergs

-3 -2 -1 0 +1 +2 +3

FIG 19 DISPLACEMENT - CENTRAL POSITION X



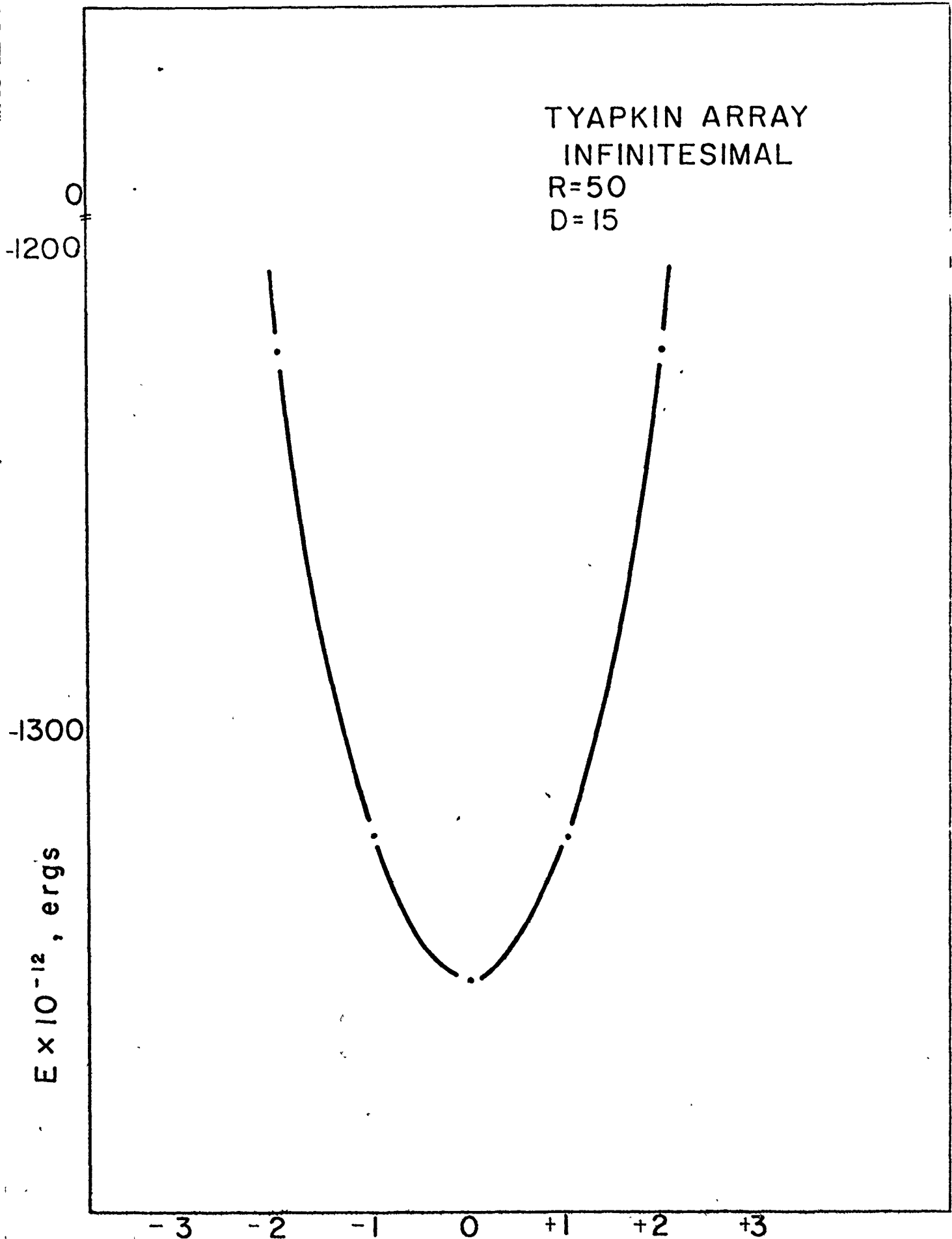


FIG.20 DISPLACEMENT OF CENTRAL PLATE  $\Delta Z$

during displacement of the central plate from its central position.

The cause of this quite opposite conclusion is apparent because the interaction potentials for two finite precipitates in the perpendicular configuration possess a minimum, (which is not the case with the potentials in infinitesimal approximation), as shown and discussed in relation to Figs. 8 - 11.

As already mentioned Eurin et al<sup>36</sup> have studied various possible arrays of precipitates. They further attributed the formation of these arrays to the elastic interactions associated with cubic-tetragonal transformation strains.

We have chosen some arrays and calculated their elastic energies by considering the interaction energies of finite precipitates. The chosen lattices are schematically represented in Fig. 21 and their corresponding energies are tabulated in table II.

All arrays listed in table II were characterized by the precipitates of the same aspect ratio and the same Burgers vector ( $1000 \times 1000 \times 100 \text{ \AA}$ ,  $b = 4 \text{ \AA}$ ).

The  $\langle 3121 \rangle$  and  $\langle 3213 \rangle$  arrays are shown in Figs. 22 and 23.

The precipitates are placed in a simple cubic lattice of parameter  $d/2$ , forming four sublattices of centres  $\alpha_i$  ( $i=1,2,3,4$ ) having cubic symmetry of the

---

\*  $b = \epsilon t$ , where  $t$  is the thickness ( $100 \text{ \AA}$ ) of the precipitate and  $\epsilon$  is the constrained elastic mismatch ( $4 \times 10^{-2}$ ).

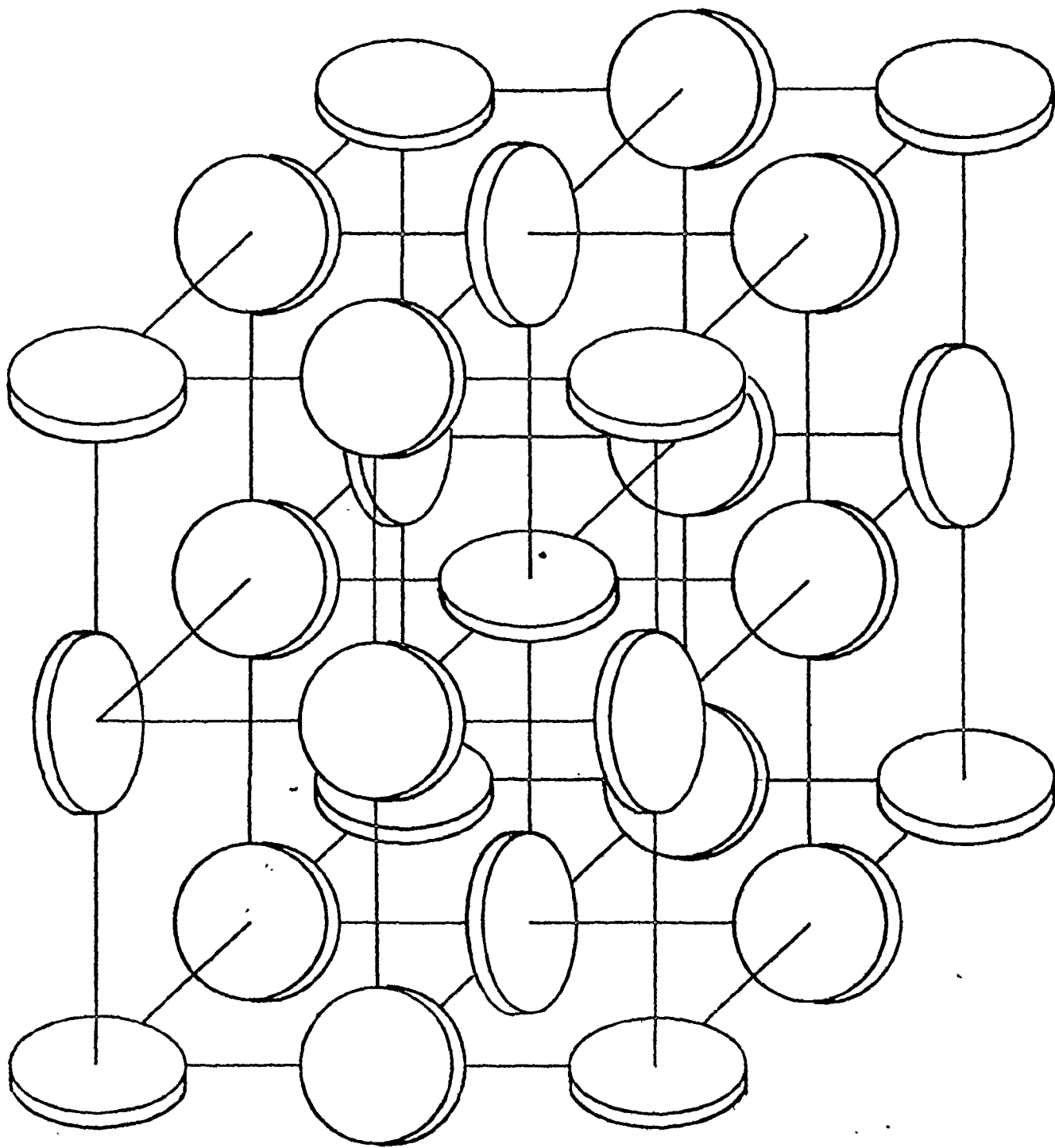


FIG. 22

<3121> ARRAY

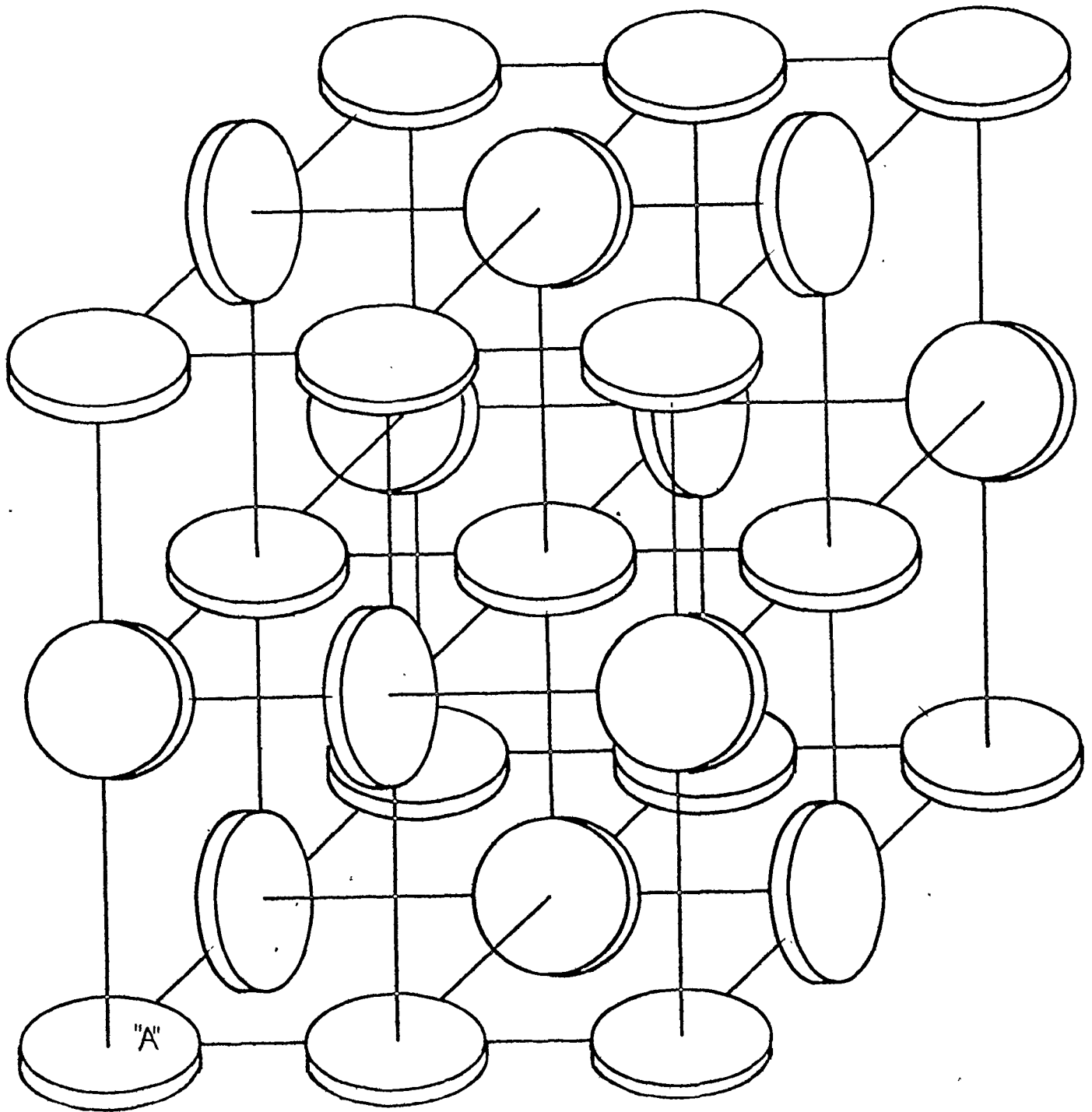


FIG.23

$\langle 3213 \rangle$  ARRAY



same parameter  $d$ .

The notation  $\langle 1 \rangle \langle 2 \rangle$  and  $\langle 3 \rangle$  in Fig. 21 denotes those precipitates whose tetragonal axes coincide with  $[100]$ ,  $[010]$  and  $[001]$  crystallographic axes, respectively.

Table II

configuration of array $\alpha_1 \alpha_2 \alpha_3 \alpha_4$	energy per unit volume ergs $\times 10^4$
1023	- 22.3135
3121	- 13.6695
3213	- 13.6700
1032	- 8.5225
1302	- 8.4645

By denoting some configurations with  $\langle pqrs \rangle$ , the nuclei  $\langle p \rangle \langle q \rangle \langle r \rangle$  and  $\langle s \rangle$  correspond to the sites  $\alpha_1 \alpha_2 \alpha_3$  and  $\alpha_4$  ( $p, q, r, s = 1, 2, 3$ ). For example, the configuration  $\langle 1210 \rangle$  represents the precipitates  $\langle 1 \rangle$  placed at sites  $\alpha_1$  and  $\alpha_3$ ,  $\langle 2 \rangle$  the precipitates placed at site  $\alpha_2$  while the site  $\alpha_4$  is not filled. The total interaction energy was calculated for the precipitates enclosed by a sphere

of radius of 50 units whereas the distance between precipitates was taken as 15 units.

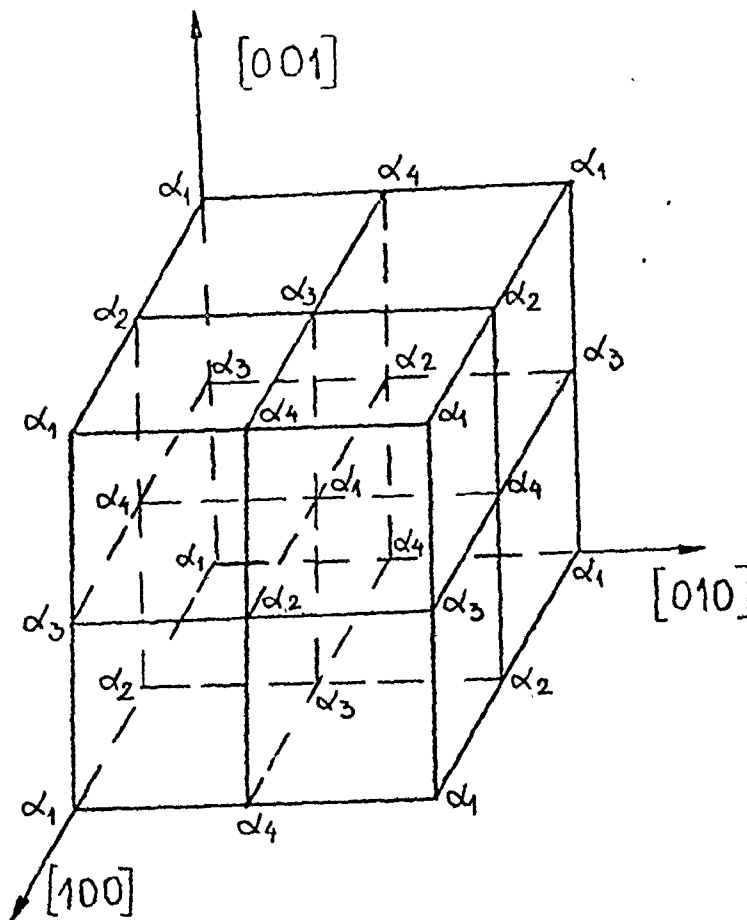


FIG. 21

From all various arrays listed in table II only the Tyapkin array possesses the property that the environment of each precipitate is identical to that of every other precipitate. To calculate the total energy

per unit volume of all arrays listed in table II, it was necessary to take into account how many precipitates possess a given environment and how many such configurations exist.

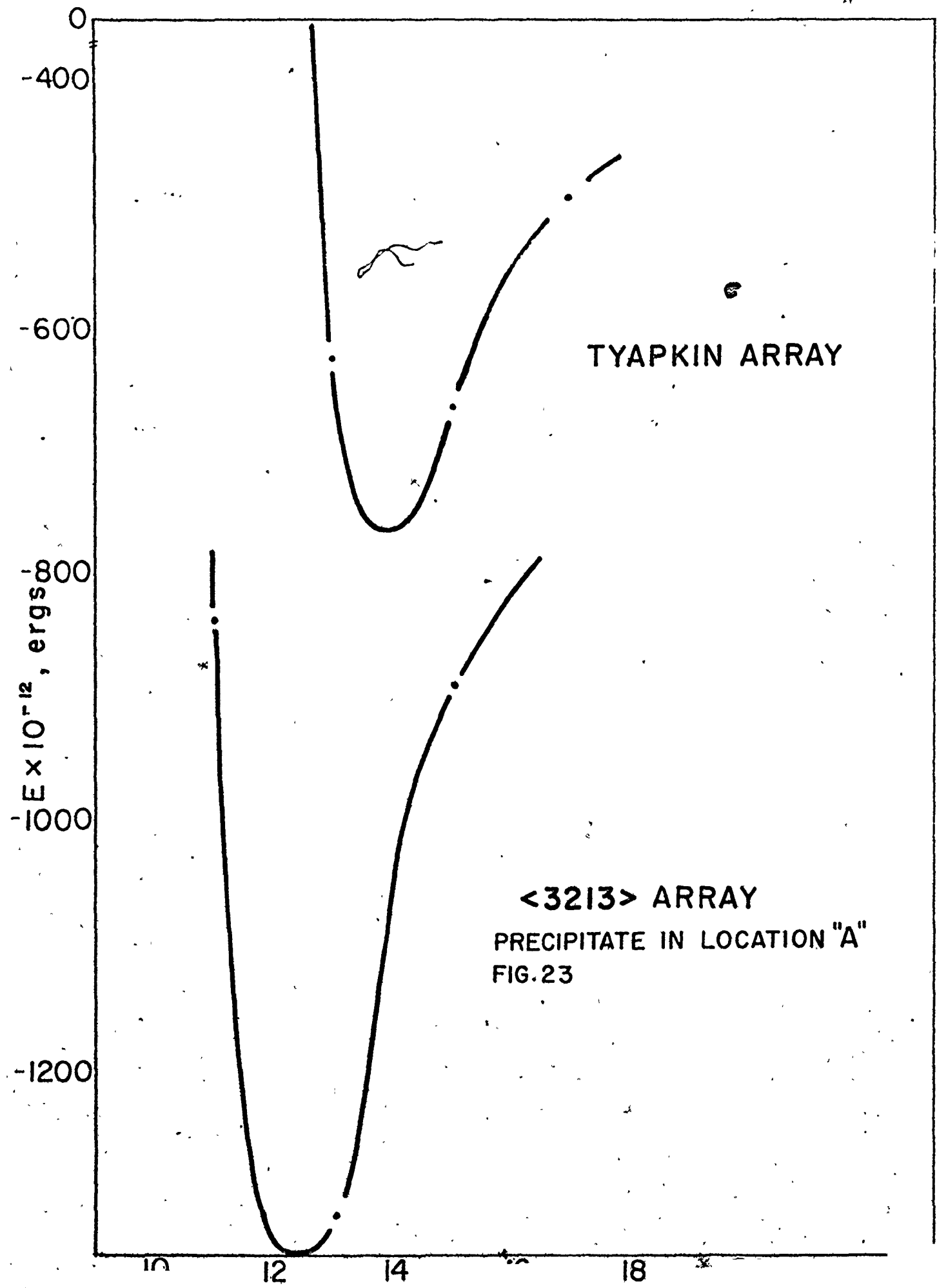
The results listed in table II show that the elastic energy depends strongly on configuration and that it can be minimized in arrays which avoid strongly repulsive interactions between neighbouring precipitates.

The distance of 15 units between the precipitates taken in calculating the interaction energies given in table II was chosen on the basis of the Tyapkin array as the most stable for that particular distance.

However, some lattices could further minimize the elastic energy by decreasing the distance between the precipitates, as shown in Fig. 24. The elastic energy of the Tyapkin array is also shown on the same figure for comparison.

The total number of precipitates enclosed by sphere of radius of 50 units for separations of 11, 13, 15 and 17 units belonging to the Tyapkin array and the  $\langle 3213 \rangle$  array are shown in the table III. It should be emphasized that the energy of the  $\langle 3213 \rangle$  array shown in Fig. 24 is the energy of a plate in the most favourable configuration and not the energy of the array.

The total interaction energy per mole of the Tyapkin array containing precipitates characterized by



1000x1000x100 Å dimensions and by Burgers vector of 4 Å, is 0.03725 cal.

By increasing the Burgers vector to 10 Å, the precipitate volume remaining the same (1000x1000x100, Å) the interaction energy was increased to 0.238 cal.

Table III

array	number of particles			
	distance(centre to centre)			
	11	13	15	17
Tyapkin		186	130	96
3213 <sub>type A</sub>	384	250	170	

The total interaction energy of a particular array is constant for given volume fraction and given aspect ratio and misfit.

The interaction energy per plate is not constant for given volume fraction and given aspect ratio, for it is proportional to the volume of the precipitate. For instance, this energy is  $-6.694 \times 10^{-13}$  ergs for precipitates characterized by the dimensions of 100x100x10, Å and by Burgers vector of 0.4 Å.

By increasing the precipitate volume by 1000 times retaining the same aspect ratio ( $1000 \times 1000 \times 100$ , Å,  $b = 4$  Å), the interaction energy becomes  $-6.694 \times 10^{-10}$  ergs. By increasing Burgers vector to  $10$  Å for the same volume of precipitates ( $1000 \times 1000 \times 100$ , Å), the interaction energy becomes more negative, i.e.  $-4.18 \times 10^{-9}$  ergs.

These facts become important when considering Ostwald ripening between two precipitates when the surface energy decrease is also very small. For example, by decreasing the volume of one precipitate by  $5\%$  in respect to the other one, the surface energy diminution due to the Ostwald ripening is only  $2.3 \times 10^{-11}$  ergs (both precipitates have had the dimensions of  $1000 \times 1000 \times 100$ , Å).

As emphasized above, the elastic energy tends to stabilize the precipitates of the same size, while the surface energy is a maximum then.

In order to investigate the stability of a regular lattice against Ostwald ripening the variation of the elastic energy of the Tyapkin array with small volume exchanges between neighbouring precipitates was investigated.

The change of the elastic energy for volume transfer between one pair of neighbouring precipitates along the  $x$  or  $y$  axis was calculated. The corresponding calculation was then performed for mass transfer in the  $z$  direction. The volume perturbation was carried out

at fixed aspect ratio. First, the energy change of the isolated pair of neighbouring precipitates was calculated. The results are given in Fig. 25 and Fig. 26. Fig. 25 shows that in the case of the edge-edge configuration (x, y - direction) the elastic energy is minimal if the precipitates are of the same size. Thus, the elastic interaction appears as a factor which stabilizes equal dimensions of the particles, if this interaction is attractive<sup>15</sup>. Fig. 26 shows the change of the elastic energy due to volume changes between the pair of precipitates in the face-face configuration (z -direction).

If the interaction is repulsive ( $E_{int}$  is positive), then it tends to promote the diffusional growth of one precipitate at the expense of the other.

From the interaction energies of pairs of precipitates (as a function of volume perturbation) it might be then concluded that the Tyapkin lattice is stable with respect to volume perturbations in the x( y ) direction but not in the z direction.

This conclusion, however, would be reached without considering the possible stabilizing influence of the lattice against the volume transport in the z direction. This possibility might come from the fact that the first nearest neighbours of the Tyapkin lattice are in the edge-edge configuration with negative interaction energies which, as shown in Fig. 25, have a stabilizing

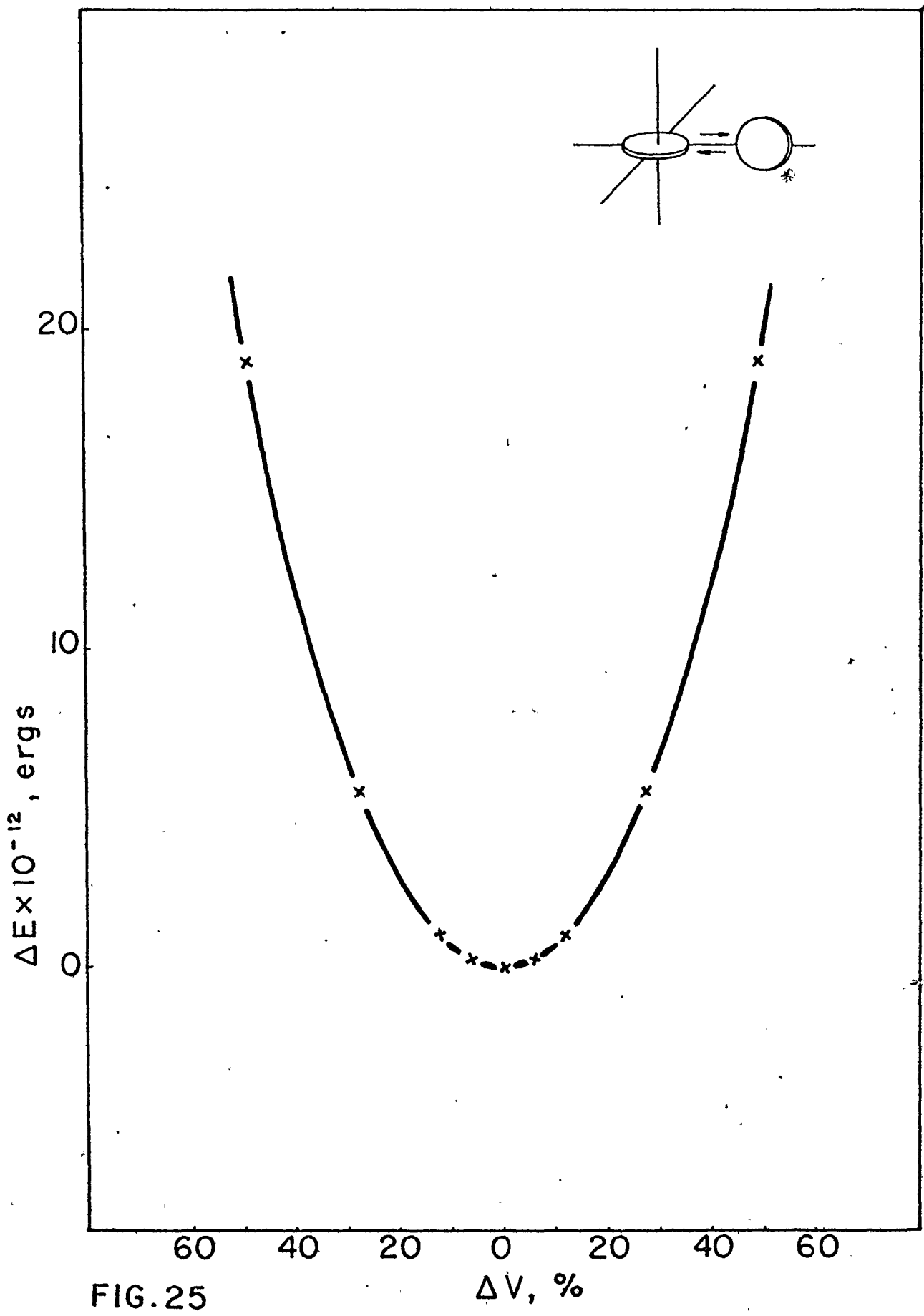


FIG. 25

$\Delta V, \%$

$\Delta E \times 10^{-12}, \text{ ergs}$



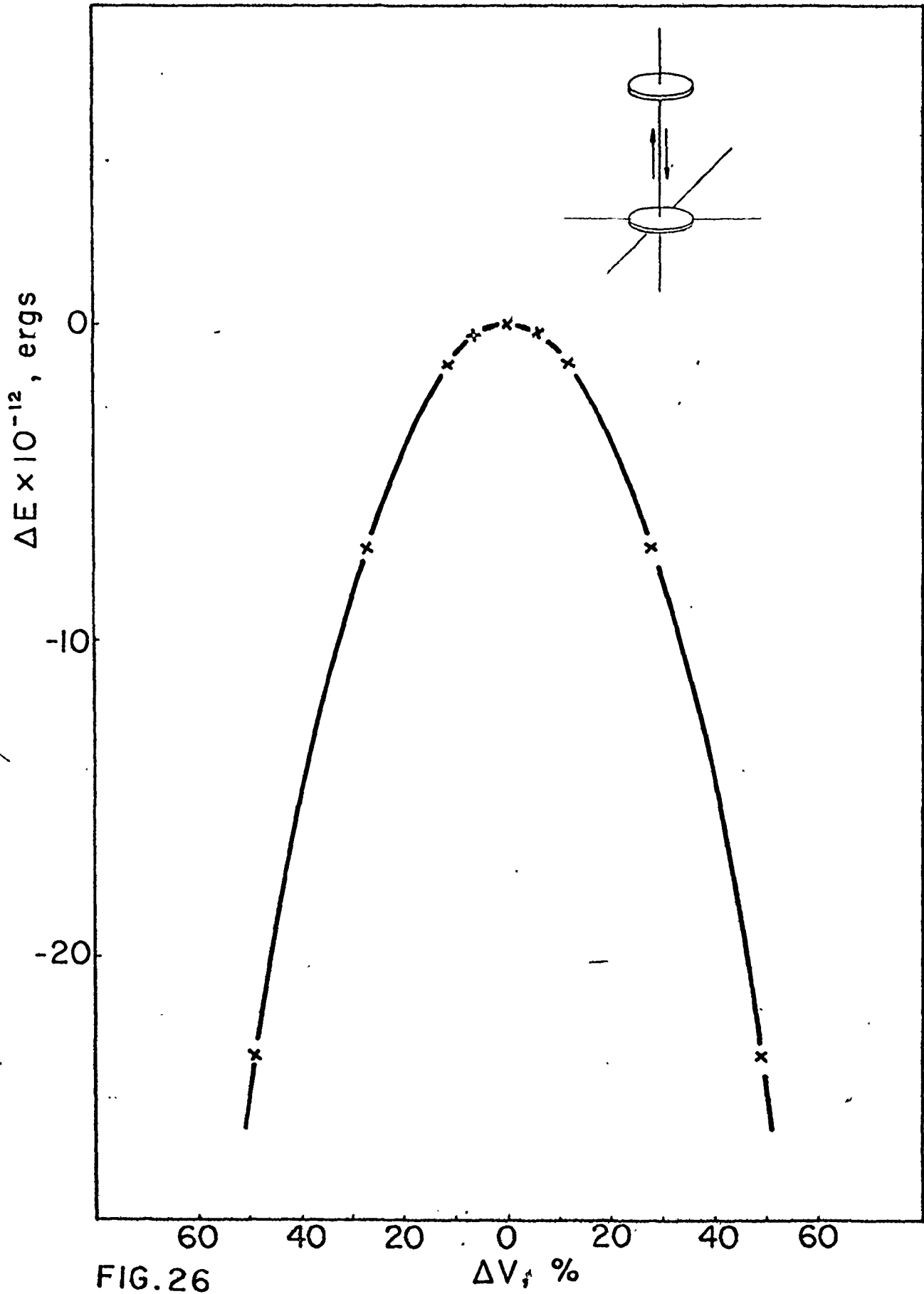


FIG. 26

effect, while the second order neighbours in the  $z$  direction have the opposite effect.

In order to investigate the stability of the pair in the strain field of the lattice, the following calculations were done:

- The total interaction energy per plate for equal size (perfect) precipitates surrounded by a interaction sphere of radius of 60 units, of precipitates spaced 15 units apart was calculated.
- The energy of the perfect lattice ( $\Delta V = 0$ ) was calculated and compared with an imperfect one, with the same number of precipitates.

The elastic energy of the imperfect lattice was calculated in the following way:

Fig. 27 shows two unequal precipitates, and the lattice of plates that interacts with this pair. The precipitates of the same distance and the same environment are marked with the same number. For example, the interaction for plate 1 was obtained by replacing equal sized precipitates 1 and 2 by unequal sized plates 1' and 2'. The energy per plate (work to form the plate in the strain field of the other plate) is given by the summation:

$$E_{\text{int}(1')} = \sum E_{\text{int}(1',-L)} - E_{\text{int}(1',-2)} + E_{\text{int}(1',-2')}$$

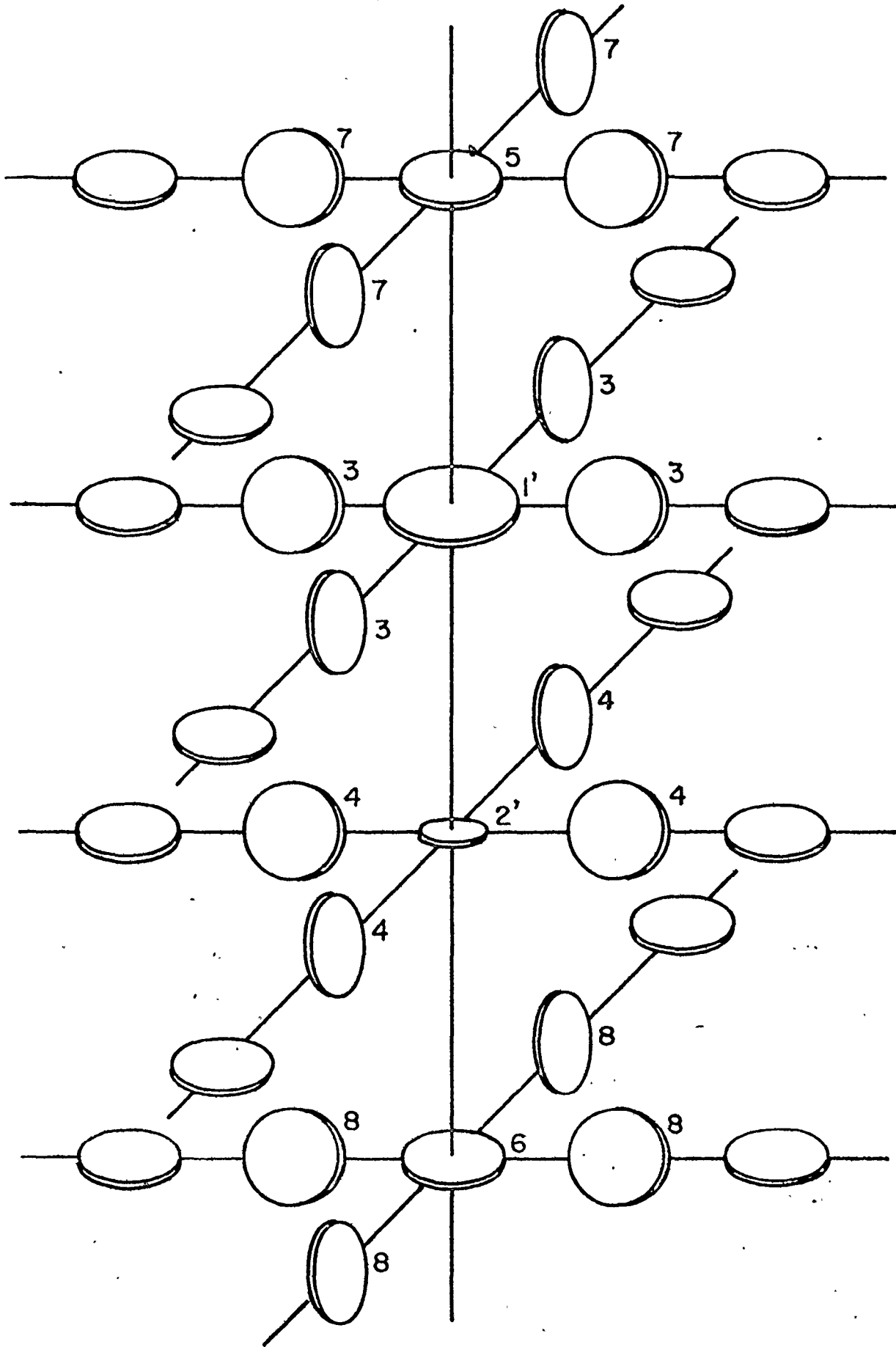


FIG.27

where  $\sum E_{\text{int}(1',-L)}$  is the sum of interactions of the unperturbed precipitates with the enlarged plate 1'. The summation was done for the precipitates enclosed by the sphere of radius of 60 units (giving 192 precipitates).  $E_{\text{int}(1',-2)}$  is the interaction energy between the enlarged precipitate 1' and the unperturbed precipitate 2'.  $E_{\text{int}(1',-2')}$  is the interaction energy between the enlarged precipitate 1' and the diminished precipitate 2'.

The total energy per plate 2' was obtained in the same way but with the imperfect plate 2' taken as the central plate:

$$E_{\text{int}(2')} = \sum E_{\text{int}(2',-L)} - E_{\text{int}(2',-1)} + E_{\text{int}(2',-1')}$$

In all other cases, the central plate was unperturbed, surrounded by perfect neighbours except for precipitates 1' and 2'.

To calculate the total interaction energy per plate of some perfect precipitate, it was necessary to find the position and the distance of the imperfect precipitates 1' and 2' and to determine whether both of them or only one was enclosed by the sphere of radius of 60 units. This radius of 60 units was chosen in order

to ensure that the interactions between 2'-5 and 1'-6 were included. (In other words, it was desirable to make sure that the most unstable configurations were taken into account in calculating the total interaction energy of the imperfect lattice).

The total interaction energy per plate 3 was obtained in the following way:

$$E_{\text{int}}(3) = \sum E_p - E_{\text{int}}(3-1) + E_{\text{int}}(3-1') - E_{\text{int}}(3-2) + E_{\text{int}}(3-2')$$

where  $\sum E_p$  is the total interaction energy per plate when all precipitates are of the same size.  $E_{\text{int}}(3-1)$  is the interaction energy of the pair of the perfect precipitates 3 and 1.  $E_{\text{int}}(3-1')$  is the interaction energy between the perfect central precipitate 3 and the imperfect precipitate 1'.  $E_{\text{int}}(3-2)$  is the interaction energy between the pair of perfect precipitates 3 and 2.  $E_{\text{int}}(3-2')$  is the interaction energy between the perfect central precipitate 3 and the imperfect precipitate 2'. Similarly, the total interaction energy per plate 4 is:

$$E_{\text{int}}(4) = \sum E_p - E_{\text{int}}(4-2) + E_{\text{int}}(4-2') - E_{\text{int}}(4-1) + E_{\text{int}}(4-1')$$

In the total interaction energy per plate 7 and 8 only one imperfect precipitate was enclosed:

$$E_{\text{int}}(7) = \sum E_p - E_{\text{int}}(7-1) + E_{\text{int}}(7-1')$$

and

$$E_{\text{int}}(8) = \sum E_p - E_{\text{int}}(8-2) + E_{\text{int}}(8-2')$$

The interaction energies of the other pairs were calculated in the analogous way.

The total energy of the imperfect lattice was obtained by summing the interaction energies of each plate with the lattice. The total energy of the perfect lattice was compared with this value.

The results of these calculations are shown in Fig. 28. It is seen that the volume perturbations in the  $z$  direction lead to an increase in the total energy of the lattice, in spite of the strong positive interaction energy of the pair of precipitates in the face-face configuration.

On the basis of the results shown in Fig. 28 it is tentatively concluded that the lattice has a stabilizing effect in respect to these volume perturbations.

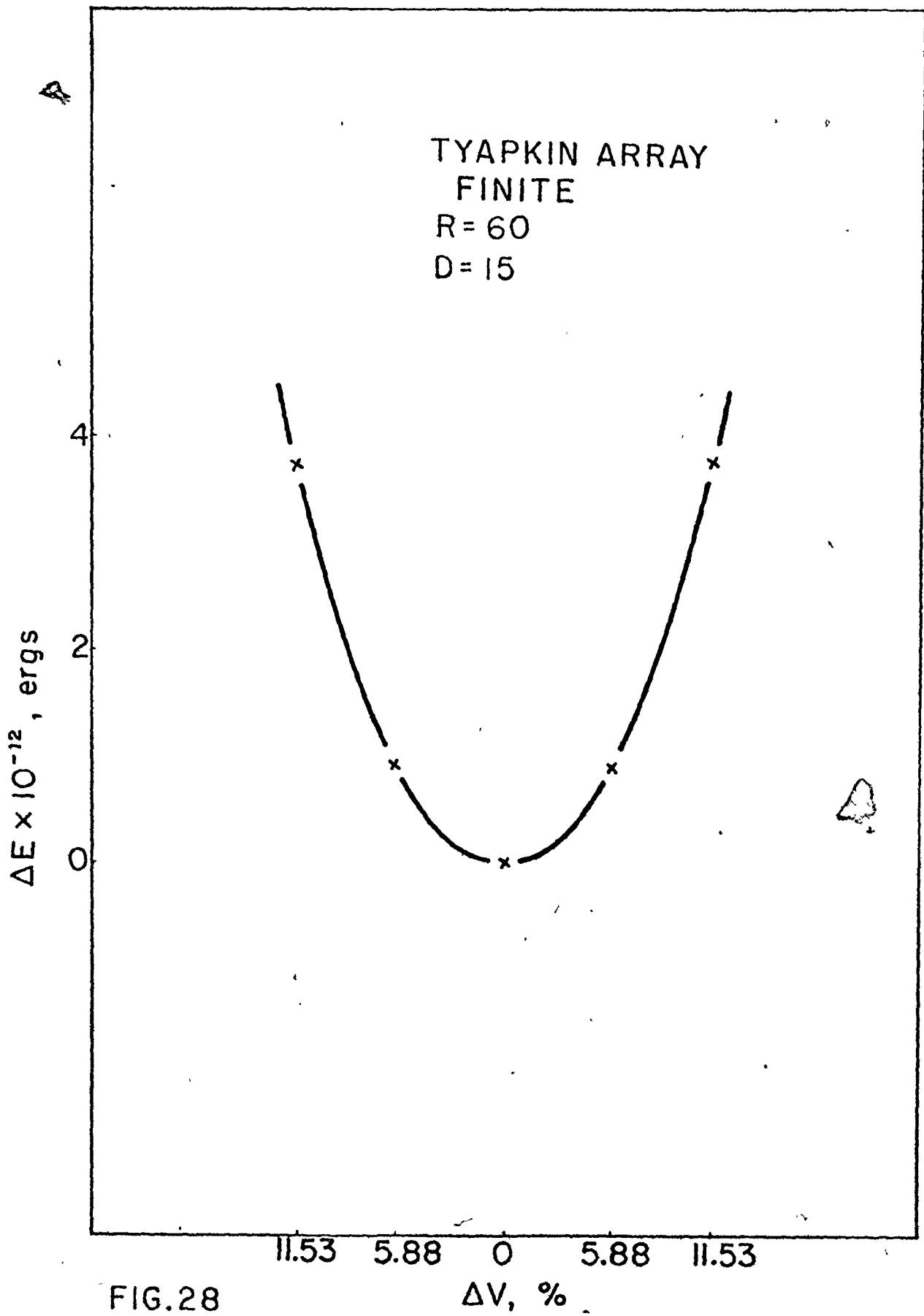


FIG.28

A detailed analysis of all interaction energies show that the biggest stabilizing contribution comes from the nearest neighbours in the edge-face configuration, as shown in Fig. 25. As already mentioned, the equilibrium is metastable, because  $E_{\text{surface}}$  has infinite slopes for  $V_1 = 0$  and for  $V_2 = 0$ : thus, a large fluctuation will cause one precipitate to grow at the expense of the other.

Testing of the Tyapkin lattice in  $x(y)$  direction was not done because it is obvious that the lattice is stable in these directions, for the first nearest neighbours are in the edge-edge configuration which is stable with respect to the volume perturbation, in accordance with the above discussion.

It is interesting to note that the same result is obtained for  $\Delta E$ , when the pairwise interactions of all precipitates (within the sphere of radius of 60 units) with the precipitates 1' and 2' are summed. This result is presumably due to the mutual cancellation of interactions among unperturbed precipitates.



CHAPTER IV  
CONCLUSIONS AND SUGGESTIONS FOR  
FUTURE WORK

IV. 1. Conclusions

1. The elastic interaction among finite precipitates causing tetragonal distortions is qualitatively and quantitatively distinguishable from that for infinitesimal precipitates.
2. The difference between the elastic energy of finite precipitates and of precipitates in infinitesimal approximation comes from the interaction of the elements far away from the centres of precipitates.  
This "peripheral" interaction causes a minimum in the interaction energy when two precipitates are mutually perpendicular, while in the parallel configuration it leads to considerable decrease of the interaction energy (otherwise positive).
3. The appearance of the minimum on the interaction curves leads to stability of the Tyapkin tridimensional array.
4. The optimum separation of square precipitates is seen to occur at a separation (centre to

- centre) of about 1.5 times the edge length.
5. Quite the opposite result was obtained from calculations based on the infinitesimal approximation.
  6. Further minimization of the elastic energy may possibly be achieved by choosing different configurations and by varying the distance between neighbouring precipitates.
  7. The greatest contribution in the elastic energy of an array comes from the closest neighbours ( $\epsilon \sim 1/r^3$ ).
  8. It was shown that the Tyapkin array is mechanically stable since any displacement of the central precipitate in either the  $x$  ( $y$ ) or  $z$  direction leaves the system in the higher energy state.
  9. The investigations of the Tyapkin array via the displacement of the central loop in infinitesimal approximation have shown this array to be unstable. The reason for this lies in the elastic energy curve versus distance in infinitesimal approximation which does not possess a minimum.
  10. The investigations of the stability on the volume perturbations between the nearest neighbours of the Tyapkin lattice in  $x$  ( $y$ ) and  $z$  di-

rections show that the edge-face configuration ( x and y directions ) is stable with respect to these volume perturbations, while the face-face pair configuration ( z direction ) is the unstable one. The reason for this lies in the fact that the edge-face configuration is attractive while the face-face configuration is repulsive.

11. The investigation of the variation of the total elastic energy of the Tyapkin array caused by volume exchange between the nearest neighbours in the z direction (the face-face configuration) shows that the lattice has a stabilizing effect. The lattice therefore possesses the minimum elastic interaction energy when all precipitates are of the same dimensions.
12. Besides detailed investigation of the Tyapkin array, the elastic energies of the other arrays were calculated and it was shown that they were less stable than the Tyapkin array. They have not been tested for stability against small perturbations.

#### IV. 2. SUGGESTION FOR FUTURE WORK

The theoretical considerations presented here have shown that regular arrangements of precipitates may lower the elastic energy of the system.

Of primary importance is the need for some experimental investigations to show that  $\Theta'$  precipitates in Al-Cu alloy are arranged in a regular array which minimizes the elastic energy of the system as a whole. That it is possible to get long range periodic arrangements of  $\Theta'$  precipitates in Al-Cu alloy is clear from Fig. 29. This electron micrograph was taken by C.M. Sargent.

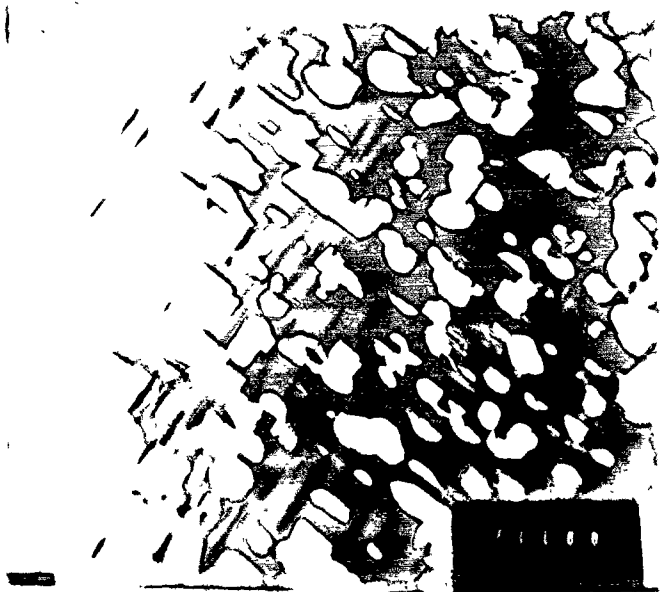
The similar periodic structure could be explained as due to an adequate tilting of some sections of the regular array of precipitates. As an example, Fig. 30 is the schematic representation of the section (110) of the  $1213$  array and of the possible effects due to slight tilting of the given section.

The most suitable technique for solving this problem is to form images using reflections characteristic of the precipitation phase, because in this case (as distinct from the bright or dark field photographs using matrix reflections) the image is not obscured by the effects connected with elastic deformations of the matrix.

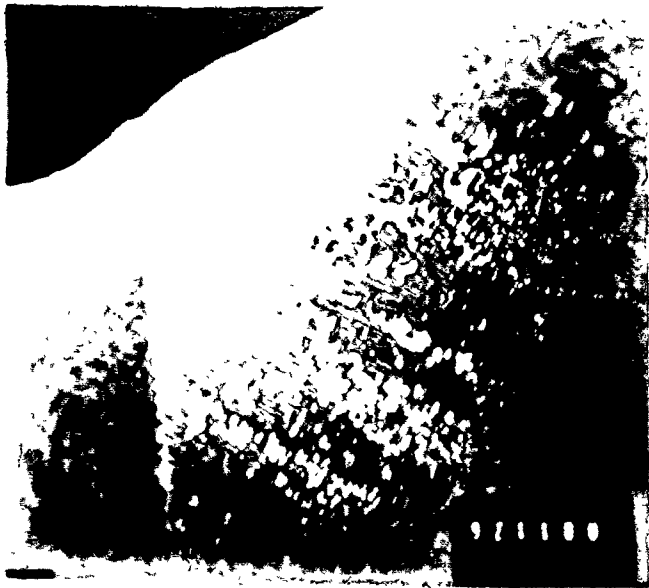
Simultaneously with experiments to determine



10500 x



10500 x



3000 x

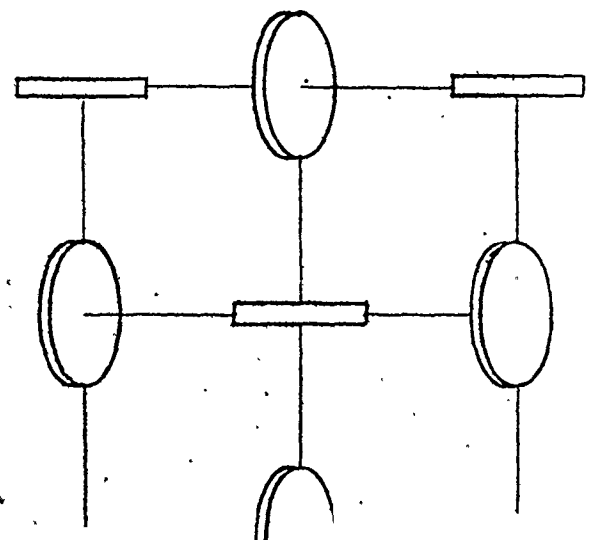
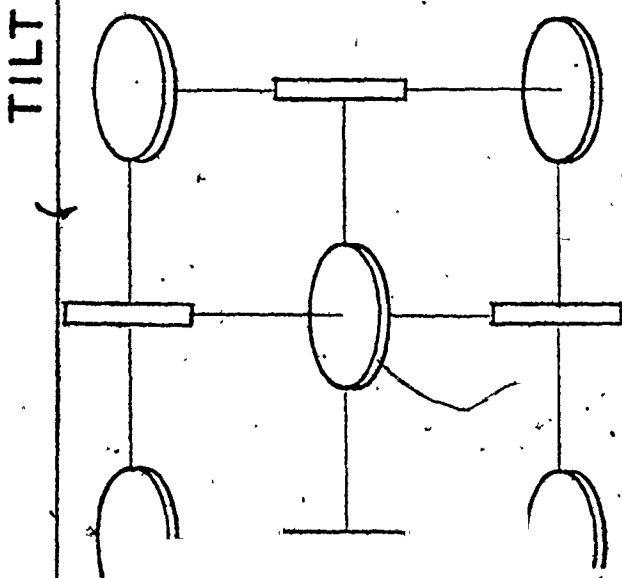
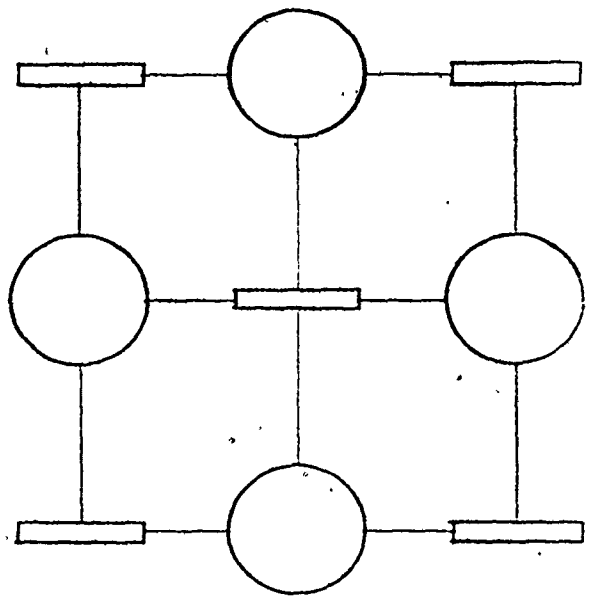
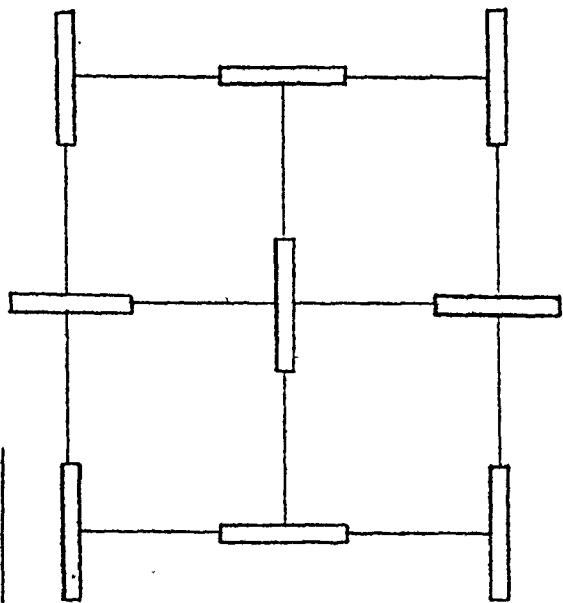
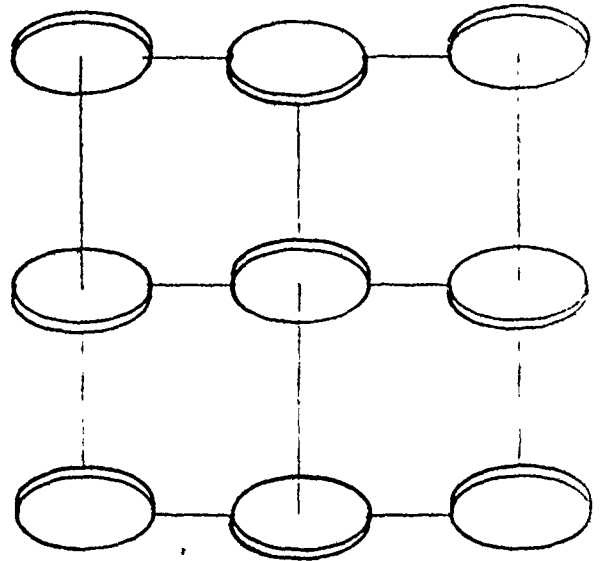
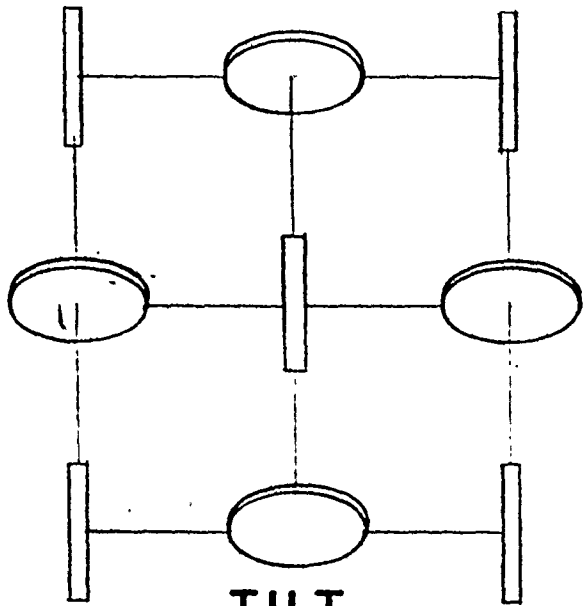


10500 x

Fig. 29. ( Courtesy of C. Sargent )

**<1213> ARRAY**

**(110) SECTION**



the spatial distribution of the precipitated phase in aging of Al-4% Cu alloy, an investigation upon the influence of the external stress on the morphology and kinetics of coarsening of precipitates would be expected to give valuable data regarding the stability of the array.

APPENDIX

Computation of interaction energies

Program 1:

```
C INTERACTION ENERGY OF TWO SQUARE PLATE SHAPED PARTICLES
C IN THE FACE-FACE CONFIGURATION AS A FUNCTION OF
C SEPARATION
  DIMENSION STE1(20),STE2(20),STE3(20),STE4(20),
  X1(20),X2(20),Y1(20),Y2(20),Z2(50)
  READ(5,500)(Z2(LZ2),LZ2=1,12)
500 FORMAT(12F5.1)
  READ(5,501)X1INI
501 FORMAT(F10.1)
  S=1.0
  M=9
  Z1=0.0
  X1(1)=X1INI
  DO 10 I=1,M
  X1(I+1)=X1(I)+S
10 CONTINUE
  N=M+1
  DO 20 I=1,N
  X2(I)=X1(I)
  Y1(I)=X1(I)
  Y2(I)=X1(I)
20 CONTINUE
  DO 200 LZ2=1,12
  STE1(1)=0.0
  STE2(1)=0.0
  STE3(1)=0.0
  STE4(1)=0.0
```



```

DO 210 LX1=1,N
DO 220 LX2=1,N
DO 230 LY1=1,N
DO 240 LY2=1,N
VX=X2(LX2)-X1(LX1)
VY=Y2(LY2)-Y1(LY1)
VZ=Z2(LZ2)
SR=VX**2+VY**2+VZ**2
R=SQRT(SR)
VA=Z2(LZ2)**2
VB=18.0*VA/SR
VC=45.0*VA**2/SR**2
VD=3.0+VB-VC
VE=(-1.9E-7/(SR*R))*VD
STE4(LY2+1)=STE4(LY2)+VE
240 CONTINUE
STE3(LY1+1)=STE3(LY1)+STE4(N)
230 CONTINUE
STE2(LX2+1)=STE2(LX2)+STE3(N)
220 CONTINUE
STE1(LX1+1)=STE1(LX1)+STE2(N)
210 CONTINUE
WRITE(6,600)Z2(LZ2),STE1(N)
600 FORMAT(1H ,10X,2HD=,F5.1,2X,5H*****,13HTOTAL ENERGY=,E15.7)
200 CONTINUE
STOP
END

```

Program 2:

```

C INTERACTION ENERGY OF TWO SQUARE PLATE SHAPED PARTICLES
C IN THE EDGE-FACE CONFIGURATION AS A FUNCTION OF SEPARATION
DIMENSION STE1(40),STE2(40),STE3(40),STE4(40),
1 X1(40),Y1(40),YC(40),Z2(40)
READ(5,500)(YC(I),I=1,12)
500 FORMAT(12F5.1)

```

```

X0=-5.5
DO 10 K=1,10
X1(K)=X0+K
Y1(K)=X1(K)
Z2(K)=X1(K)

```

10 CONTINUE

```

DO 200 I=1,12
STE1(1)=0.0
STE2(1)=0.0
STE3(1)=0.0
STE4(1)=0.0
DO 210 LX1=1,10
DO 220 LY2=1,10
DO 230 LY1=1,10
DO 240 LZ2=1,10
VP=YC(I)-5.5+LY2
VY=VP-Y1(LY1)
VX=X1(LX1)
VZ=Z2(LZ2)
SR=VX**2+VY**2+VZ**2
R=SQRT(SR)
VA=VP**2+Z2(LZ2)**2
VB=VP*Z2(LZ2)
VC=3.0*VA/SR
VD=45.0*VB**2/SR**2
VE=1.0+VC-VD
VF=(-1.9E-7/(SR*R))*VE
STE4(LZ2+1)=STE4(LZ2)+VF

```

240 CONTINUE

```

STE3(LY1+1)=STE3(LY1)+STE4(10)

```

230 CONTINUE

```

STE2(LY2+1)=STE2(LY2)+STE3(10)

```

220 CONTINUE

```

STE1(LX1+1)=STE1(LX1)+STE2(10)

```

```

210 CONTINUE
      WRITE(6,600)YC(I),STE1(10)
600 FORMAT(1H ,10X,2HD=,F5.1,2X,5H*****,13HTOTAL ENERGY=E15.7)
200 CONTINUE
      STOP
      END

```

Program 3:

```

C   THE TYAPKIN ARRAY (THE FINITE APPROXIMATION) - VERTICAL
C   PLATES-
      DIMENSION STE1(300),STE2(300),STE3(300),STE4(300),
1  X1(300),Y1(300),XC(300),YC(300),ZC(300)
      READ(5,500)(XC(I),I=1,N)
500 FORMAT(NF5.1)
C   N IS A FUNCTION OF THE VOLUME FRACTION FOR A GIVEN ARRAY
      READ (5,501)(YC(I),I=1,N)
501 FORMAT (NF5.1)
      READ(5,502)(ZC(I),I=1,N)
502 FORMAT(NF5.1)
      XO=-5.5
      DO 10 K=1,10
      X1(K)=XO+K
      Y1(K)=X1(K)
10 CONTINUE
      SUME=0.0
      DO 190 I=1,N
      XX=XC(I)
      YY=YC(I)
      ZZ=ZC(I)
      SRI=XX**2+YY**2+ZZ**2
      RI=SQRT(SRI)
      IF(RI-100.0)11,11,190
11 DO 200 KX=1,10
      DO 210 KY=1,10
      DO 220 JX=1,10
      DO 230 JZ=1,10

```

```
STE1(1)=0.0
STE2(1)=0.0
STE3(1)=0.0
STE4(1)=0.0
VP=XC(I)-5.5+JX
VR=ZC(I)-5.5+JZ
VX=VP-X1(KX)
VZ=VR
VY=YC(I)-Y1(KY)
SR=VX**2+VY**2+VZ**2
R=SQRT(SR)
VA=VP**2+VR**2
VB=VP*VR
VC=3.0*VA/SR
VD=45.0*VB**2/SR**2
VE=1.0+VC-VD
VF=(-1.9E-7/(SR*R))*VE
STE4(JZ+1)=STE4(JZ)+VF
230 CONTINUE
STE3(JX+1)=STE3(JX)+STE4(10)
220 CONTINUE
STE2(KY+1)=STE2(KY)+STE3(10)
210 CONTINUE
STE1(KX+1)=STE1(KX)+STE2(10)
200 CONTINUE
WRITE(6,600)STE1(10)
600 FORMAT(1H,5X,13HTOTAL ENERGY=,E15.7)
SUME=SUME+STE1(10)
WRITE(6,700)SUME
700 FORMAT(1H,5X,12HSUME ENERGY=,E15.7)
190 CONTINUE
STOP
END
```

Program 4:

```

C     THE TYAPKIN ARRAY (THE FINITE APPROXIMATION) - PARALLEL
C     PLATES -
      DIMENSION STE1(300),STE2(300),STE3(300),STE4(300),
1     X1(300),Y1(300),XC(300),YC(300),ZC(300)
      READ(5,500)(XC(I),I=1,N)
500  FORMAT(NF5.1)
C     N IS A FUNCTION OF THE VOLUME FRACTION FOR A GIVEN ARRAY
      READ(5,501)(YC(I),I=1,N)
501  FORMAT(NF5.1)
      READ(5,502)(ZC(I),I=1,N)
502  FORMAT(NF5.1)
      XO=-5.5
      DO 10 K=1,10
      X1(K)=XO+K
      Y1(K)=X1(K)
10   CONTINUE
      SUME=0.0
      DO 190 I=1,N
      XX=XC(I)
      YY=YC(I)
      ZZ=ZC(I)
      SRI=XX**2+YY**2+ZZ**2
      RI=SQRT(SRI)
      IF(RI-100.0)11,11,190
11  DO 200 KX=1,10
      DO 210 KY=1,10
      DO 220 JX=1,10
      DO 230 JY=1,10
      STE1(1)=0.0
      STE2(1)=0.0
      STE3(1)=0.0
      STE4(1)=0.0
      VP=XC(I)-5.5+JX
      VQ=YC(I)-5.5+JY
      VZ=ZC(I)

```

```

VX=VP-X1(KX)
VY=VQ-Y1(KY)
SR=VX**2+VY**2+VZ**2
R=SQRT(SR)
VA=ZC(I)**2
VB=18.0*VA/SR
VC=45.0*VA**2/SR**2
VD=3.0+VB-VC
VE=(-1.9E-7/(SR*R))*VD
STE4(JY+1)=STE4(JY)+VE
230 CONTINUE
STE3(JX+1)=STE3(JX)+STE4(10)
220 CONTINUE
STE2(KY+1)=STE2(KY)+STE3(10)
210 CONTINUE
STE1(KX+1)=STE1(KX)+STE2(10)
200 CONTINUE
WRITE(6,600)STE1(10)
600 FORMAT(1H ,5X,13HTOTAL ENERGY=,E15.7)
SUME=SUME+STE1(10)
WRITE(6,700)SUME
700 FORMAT(1H ,5X,12HSUME ENERGY=E15.7)
190 CONTINUE
STOP
END

```

Program 5:

```

C THE TYAPKIN ARRAY (THE INFINITESIMAL APPROXIMATION)
C - VERTICAL LOOPS - (D=15.0)
COMMON RRI(200),RVE(200)
DIMENSION XC(300),YC(300),ZC(300),SUME(300)
WRITE(6,500)
500 FORMAT(1H ,5X,8HDISTANCE,7X,6HENERGY,9X,13HSUM OF ENERGY/)
IJL=1
DO 5 I=1,200
RRI(I)=0.0

```

```
5 RVE(I)=0.0
DO 10 I=30,180,30
DO 20 J=30,180,30
DO 30 L=30,180,30
XO=-30.0
YO=-15.0
ZO=-15.0
XC(I)=XO+I
YC(J)=YO+J
ZC(L)=ZO+L
XX=XC(I)
YY=YC(J)
ZZ=ZC(L)
SRI=XX**2+YY**2+ZZ**2
RI=SQRT(SRI)
IF(RI-50.0)10,10,100
100 VA=YC(J)**2
VB=3.0*VA/SRI
VC=XC(I)*ZC(L)
VD=45.0*VC**2/SRI**2
VF=4.0-VB-VD
VE=(-1.9E-3/(SRI*RI))*VF
CALL ORDER(IJL,VE,RI)
IJL=IJL+1
30 CONTINUE
20 CONTINUE
10 CONTINUE
SUME(1)=RVE(1)
IJ=IJL-1
DO 50 I=1,IJ
50 SUME(I+1)=SUME(I)+RVE(I+1)
WRITE(6,600)(RRI(I),RVE(I),SUME(I),I=1,IJL)
600 FORMAT(5X,3E15.7)
STOP
END
```

```

SUBROUTINE ORDER(IJL,VE,RI)
DIMENSION TRI(200),TVE(200)
COMMON RRI(200),RVE(200)
DO 100 I=1,IJL
  IF(RRI(I)-RI)10,20,20
20 DO 5 J=1,IJL
  TRI(J)=0.0
  5 TVE(J)=0.0
  DO 30 J=I,IJL
  TRI(J-I+1)=RRI(J)
30 TVE(J-I+1)=RVE(J)
  RRI(I)=RI
  RVE(I)=VE
  IT=IJL-I+1
  DO 40 J=1,IT
  RRI(I+J)=TRI(J)
40 RVE(I+J)=TVE(J)
  RETURN
10 IF(I.EQ.IJL) GO TO 200
100 CONTINUE
200 RRI(IJL)=RI
  RVE(IJL)=VE
  RETURN
END

```

Program 6:

```

C   THE TYAPKIN ARRAY (THE INFINITESIMAL APPROXIMATION)
C   - PARALLEL LOOPS - (D=15.0)
COMMON RRI(200),RVE(200)
DIMENSION XC(300),YC(300),ZC(300),SUME(300)
WRITE(6,500)
500 FORMAT(1H ,5X,8HDISTANCE,7X,6HENERGY,9X,13HSUM OF ENERGY/)
  IJL=1
  DO 5 I=1,200
  RRI(I)=0.0
  5 RVE(I)=0.0
  DO 10 I=30,180,30

```



```
DO 20 J=30,180,30
DO 30 L=30,180,30
X0=-30.0
Y0=-30.0
Z0=-30.0
XC(I)=X0+I
YC(J)=Y0+J
ZC(L)=Z0+L
XX=XC(I)
YY=YC(J)
ZZ=ZC(L)
SRI=XX**2+YY**2+ZZ**2
RI=SQRT(SRI)
IF(RI-50.0)10,10,100
100 VA=ZC(L)**2
VB=18.0*VA/SRI
VC=45.0*VA**2/SRI**2
VD=3.0+VB-VC
VE=(-1.9E-3/(SRI*RI))*VD
CALL ORDER(IJL,VE,RI)
IJL=IJL+1
30 CONTINUE
20 CONTINUE
10 CONTINUE
SUME(1)=RVE(1)
IJ=IJL-1
DO 50 I=1,IJ
50 SUME(I+1)=SUME(I)+RVE(I+1)
WRITE(6,600)(RRI(L),RVE(I),SUME(I),I=1,IJL)
600 FORMAT(5X,3E15.7)
STOP
END
SUBROUTINE ORDER(IJL,VE,RI)
DIMENSION TRI(200),TVE(200)
COMMON RRI(200),RVE(200)
```

```

DO 100 I=1,IJL
  IF(RRI(I)-RI)10,20,20
20 DO 5 J=1,IJL
  TRI(J)=0.0
  5 TVE(J)=0.0
  DO 30 J=I,IJL
  TRI(J-I+1)=RRI(J)
30 TVE(J-I+1)=RVE(J)
  RRI(I)=RI
  RVE(I)=VE
  IT=IJL-I+1
  DO 40 J=1,IT
  RRI(I+J)=TRI(J)
40 RVE(I+J)=TVE(J)
  RETURN
10 IF(I.EQ.IJL) GO TO 200
100 CONTINUE
200 RRI(IJL)=RI
  RVE(IJL)=VE
  RETURN
END

```

Program 7:

```

C   VOLUME PERTURBATION BETWEEN TWO FINITE PLATES IN THE
C   EDGE-FACE CONFIGURATION
C   DIMENSION STE1(300),STE2(300),STE3(300),STE4(300),
1  AB1(100),AB2(100),X1I(100),Y2I(100),Z2I(100),X1(100),
1  Y1(100),Y2(100),Z2(100)
  READ(5,500)(AB1(K),K=1,4)
500 FORMAT(4F20.7)
  READ(5,501)(AB2(K),K=1,4)
501 FORMAT(4F20.7)
  READ(5,502)(X1I(K),K=1,4)
502 FORMAT(4F20.7)
  READ(5,503)(Y2I(K),K=1,4)

```

```
503 FORMAT(4F20.7)
    READ(5,504)(Z2I(K),K=1,4)
504 FORMAT(4F20.7)
    DO 150 L=1,11,5
    DO 5 K=1,4
    S=1.0
    M=9
    X1(1)=X1I(K)
    DO 10 I=1,M
    X1(I+1)=X1(I)+S+AB1(K)
10 CONTINUE
    N=M+1
    DO 20 I=1,N
    Y1(I)=X1(I)
20 CONTINUE
    Y2(1)=Y2I(K)+L-1.0
    DO 30 I=1,M
    Y2(I+1)=Y2(I)+S-AB2(K)
30 CONTINUE
    Z2(1)=Z2I(K)
    DO 40 I=1,M
    Z2(I+1)=Z2(I)+S-AB2(K)
40 CONTINUE
    STE1(1)=0.0
    STE2(1)=0.0
    STE3(1)=0.0
    STE4(1)=0.0
    DO 200 LX1=1,N
    DO 210 LY1=1,N
    DO 220 LY2=1,N
    DO 230 LZ2=1,N
    VX=X1(LX1)
    VY=Y2(LY2)-Y1(LY1)
    VZ=Z2(LZ2)
    SR=VX**2+VY**2+VZ**2
    R=SQRT(SR)
```

```
VA=Y2(LY2)**2+Z2(LZ2)**2
VB=Y2(LY2)*Z2(LZ2)
VC=3.0*VA/SR
VD=45.0*VB**2/SR**2
VE=1.0+VC-VD
VF=(-1.9E-7/(SR*R))*VE
STE4(LZ2+1)=STE4(LZ2)+VF
230 CONTINUE
STE3(LY2+1)=STE3(LY2)+STE4(N)
220 CONTINUE
STE2(LY1+1)=STE2(LY1)+STE3(N)
210 CONTINUE
STE1(LX1+1)=STE1(LX1)+STE2(N)
200 CONTINUE
WRITE(6,600)AB1(K),Y2(1),STE1(N)
600 FORMAT(1H ,5X,4HAB1=,F10.4,5X,3HY2=,F10.4,10X,7HENERGY=,E15.7)
5 CONTINUE
150 CONTINUE
STOP
END
```

REFERENCES:

1. A.G. Khachaturyan, Soviet Phys. Solid State 8, 2163 (1967)
2. M. Hillert, M. Cohen and B.L. Averbach, Acta Met. 9, 536 (1961)
3. A.H. Geisler, Trans. ASM 43, 70 (1951)
4. E. Biederman and E. Kneller, Z. Metallk., 47, 290 (1956)
5. L.E. Tanner, Phil. Mag., 14, 111 (1966)
6. A.V. Gavrilova and Yu.D. Tyapkin, Sov. Phys.-Crystallogr., 9 166 (1964)
7. J. Manenc, Acta Cryst., 10, 259 (1959)
8. J. Manenc, Acta Met., 7, 124 (1959)
9. A.J. Ardell, R.B. Nicholson and J.D. Eshelby, Acta Met., 14, 1295 (1966)
10. E. Hornbogen and M. Roth, Z. Metallk., 58, 1533 (1966)
11. T.J. Tiedema, J. Bouman and W.G. Burgers, Acta Met., 5, 310 (1957)
12. R. Davies and R.H. Richman, Trans. AIME, 236, 1551 (1966)
13. J.M. Penisson, A. Bourret and Ph. Eurin, Acta Met., 19, 1195 (1971)

14. J.D. Eshelby, Proc. Roy. Soc., A241, 376 (1957)
15. A.G. Khachaturyan and G.A. Chatalov, Soviet Phys. Solid State, 11, 118 (1969)
16. A.G. Khachaturyan, Soviet Phys. JETP., 31, 98 (1970)
17. J.W. Cahn, Inst. Metals Monogr., 33, 1 (1968)
18. J.M. Lifshitz and V.V. Slyozov, Soviet Phys. JETP., 35, 331 (1959)
19. C. Wagner, Z. Elektrochem., 65, 581 (1961)
20. J.D. Boyd and R.B. Nicholson, Acta Met., 19, 1379(1971)
21. R.K. Ham, R.H. Cook and G.R. Purdy and G. Willoughby, Met. Sci. J., 6, 203 (1972)
22. H.K. Hardy and T.J. Heal, Prog. Met. Phys., 5, 143 (1954)
23. A. Kelly and R.B. Nicholson, Prog. Mat. Sci., 10
24. A. Guinier, Ann. Phusique, 12, 161 (1939)
25. G.D. Preston, Phil. Mag., 26, 855 (1938)
26. V. Gerold, Z. Metall., 45, 593 (1954)
27. J.M. Silcock, T.J. Heal and H.K. Hardy, J. Inst. Met., 84, 23 (1953)
28. A. Guinier, J. Metals, 8, 673 (1956)
29. V. Gerold, Acta Cryst., 13, 45 (1958)
30. D.R. James and G.L. Liedl, Acta Cryst., 18, 768(1965)
31. F.R.N. Nabarro, Proc. Phys. Soc., 59, 255 (1947)
32. H. Franz and E. Kroner, Z. Metallk., 46, 639 (1955)
33. R. Bullough and R.C. Newman, Phil. Mag., 5, 921(1960)
34. F. Kroupa, Czech. J. Phys., B(10), 284 (1960)

35. F. Kroupa, *Phil. Mag.*, 7, 783 (1962)
36. P.H. Eurin, J.M. Penisson and A. Bourett,  
*Acta Met.*, 21, 559 (1973)
37. P.J. Fillingham, H.J. Leamy and L.E. Tanner,  
5<sup>th</sup> Int. Mat. Symp. U. Calif. Berkeley
38. L.M. Brown, R.H. Cook, R.K. Ham and G.R. Purdy,  
*Scripta Met.*, 7, 815 (1973)
39. A.V. Gavrilova, Yu.D. Tyapkin and M.P. Usikov,  
*Soviet Phys. - Doklady*, 12, 970 (1968)